Investigation of human brain function by applying neuroimaging techniques available in clinics

Ph.D. thesis

Tibor Auer, M.D.

University of Pécs

2008.

Supervisors: Prof. Tamás Dóczi, M.D., Ph.D., D.Sc.

Attila Schwarcz, M.D., Ph.D.

Acknowledgments

The work involved in this thesis could not have been carried out without enormous help from a number of persons, to whom I owe a great debt of gratitude and whom I would like to thank for their valuable contribution.

First, I would like to thank Prof. Tamás Dóczi and Attila Schwarcz, my supervisors, for providing me with the excellent opportunity to carry out the work for my Ph.D. thesis at the Department of Neurosurgery, University of Pécs. Their continuous support and the stimulating discussions with them furnished excellent conditions for my research, teaching me the basics of MRI and resulting in progress in the MRI methodology.

I would also like emphasize my deep gratitude towards József Janszky and Prof. Sámuel Komoly, for welcoming me to the Department of Neurology; and for providing their knowledge and insight in the field of neurology.

Many thanks are also due to Prof. Ferenc Gallyas, as being my first supporter in the field of neuroscience. The invaluable discussions with him regarding the mysteries of the living tissue in the central nervous system have given me unique thinking. Furthermore, I would like to thank Béla Németh, Ferenc Kövér and Péter Bódi at the Pécs Diagnostic Center for granting me a workplace and all the technical and financial support.

I also owe my gratitude to Prof. Jens Frahm and his colleague, Klaus-Dietmar Merboldt, at the Max Planck Institute for Biophysical Chemistry, Göttingen, Germany, for extending my know-how in MRI methods.

Last but not least, I express my gratitude to my family for their love and support.

CONTENTS

Abbreviations

α	flip Angle (of the excitation pulse)
BOLD	Blood Oxygenation Level Dependent
BW	(receiver) BandWidth
CBF	Cerebral Blood Flow
CMR	Cerebral Metabolic Rate
CT	Computerized Tomography
DBS	Deep Brain Stimulation
DTI	Diffusion Tensor Imaging
DV	Déjà Vu
DWI	Diffusion-Weighted Imaging
EEG	Electro-EncephaloGram
EPI	Echo Planar Imaging
FA	Fractional Anisotropy
FLASH	Fast Low-Angle Shot
fMRI	functional Magnetic Resonance Imaging
FOV	Field Of View
FT	Fiber Tracking
FWHM	Full Width at Half Maximum
GLM	General Linear Model
IWG	Internal Word Generation
HRF	Hemodinamical Response Function
MR	Magnetic Resonance
MRI	Magnetic Resonance Imaging

MRS	Magnetic Resonance Spectroscopy
NMR	Nuclear Magnetic Resonance
PET	Positron Emission Tomography
PFM	Passive Finger Movement
ROI	Region Of Interest
SFO	Sequential Finger Opposition
SISCOM	Subtraction Ictal SPECT Co-registered to MRI
SNR	Signal-to-Noise Ratio
SPECT	Single-Photon-Emission Computed Tomography
SPM	Statistical Parametric Mapping
T	Tesla (measure of magnetic field strength)
T_1	Longitudinal/Spin-Lattice Relaxation Time
T_2	Transversal/Spin-Spin Relaxation Time
T_2*	effective Transversal/Spin-Spin Relaxation Time
TBI	Traumatic Brain Injury
TCD	Trans-Cranial Doppler
TE	Echo Time (time between the excitation and the acquisition)
TLE	Temporal Lobe Epilepsy
TR	Repetition Time (time between two excitations)
TTC	Two-Threshold Correlation

1. Introduction

Previously, magnetic resonance imaging (MRI) in humans has been applied merely to examine anatomical and pathological macrostructure of the brain. Novel techniques, however, enable us to obtain an insight into the microstructure and to investigate and even to visualize the function of the human brain. In addition to it, we can have all the great advantage of MRI; as it is noninvasive and harmless, according to our present knowledge. The potential and applicability of these techniques have not been widely studied in Hungary because of three main reasons: (a) with very few recent exception (Philips Achieva 3T system in Budapest and Siemens TIM Trio 3T system in Pécs), there are no experimental MR systems in Hungary; (b) additionally the clinical MR scanners – they are usually operating at lower-field (0.5-1.5T) – are generally loaded with routine measurements and machine time has not been devoted to state-of-the-art experiments; (c) most researchers are convinced about that a higher field strength is unquestionably superior when applying novel techniques. This situation has resulted in a large gap in MR knowledge between Hungary and more developed countries, which is reflected in a relative lack of Hungarian publications in respected MRI related journals. However, it is not only a question of money! During my Ph.D. training, I have attempted to learn and understand a wide spectrum of novel *in vivo* MR techniques ranging from functional MRI (fMRI), diffusion-weighted imaging (DWI), volumerty and relaxometry to metabolite quantification with spectroscopy (MRS). I have also pushed hard to convince other scientists about applying these techniques also at lower-field to make them accessible widely. These new MR methods can facilitate not just human studies. It is at least so important, that they can also be of service to the patients, who can be managed better clinically, for instance at the stage of preoperative neurosurgical planning, intraoperative

functional neuronavigation or monitoring and – with the help of e.g. neurofeedback (Weiskopf et al, 2007) – intensifying their postoperative rehabilitation.

1.1. Nuclear magnetic resonance and magnetic resonance imaging

History

NMR is a phenomenon involving magnetic fields and radiofrequency electromagnetic waves. It was discovered in 1946 independently by Bloch (Bloch et al, 1946) and Purcell (Purcell et al, 1946). For their discoveries, they were awarded the Nobel Prize in 1952. Since then, it has become a useful tool, especially in analytical chemistry and biochemistry, thanks to the discovery of the chemical shift. The *in vivo* techniques of NMR make use of electromagnetic radiation to probe living tissues. The radiation has low energy and appears to be safe under normal operating conditions. The idea to extend NMR to *in vivo* studies dates back to 1968, when what are believed to be the first NMR signals from a live animal were produced (Jackson and Langham, 1968). The first two-dimensional proton NMR image of a water sample was generated in 1973, using a back projection technique (Lauterbur, 1973) similar to that used in computerized tomography (CT). This was the birth of magnetic resonance imaging (MRI), and it showed that hospitals were willing to spend a huge amount of money for medical imaging systems. In 1975, Ernst proposed MRI using phase and frequency encoding, and the Fourier Transform (Kumar et al, 1975), for which he was rewarded with Nobel Prize in 1991. A few years later, in 1977, Raymond Damadian demonstrated MRI by using "field-focusing nuclear magnetic resonance" (FONAR) (Damadian et al, 1978). He produced the first commercial scanner, called "Indomitable". With this machine it took 4 hours and 45 minutes to take a whole-body scan. In this same year, Peter Mansfield developed the echo-planar imaging (EPI)

technique (Mansfeld, 1977). Lauterbur together with Mansfield were awarded the Nobel Prize in Medicine for their discoveries in 2003. Edelstein and coworkers demonstrated imaging of the body using Ernst's technique in 1980, with which a single image could be acquired in approximately five minutes. In 1985, Frahm and coworkers succeed to shorten the measuring time by up to two orders of magnitude with Fast Low Angle Shot (FLASH) (Haase et al, 1986). Almost all novel MRI techniques are based on FLASH and/or EPI. These improvements made it possible to produce images nowadays even at video rates (30 ms / image).

Images, scans, volumes and slices

These terms are used quite often in the literature and also in my thesis. To make it clear I use the following definitions:

- slice: one sample of 2D dataset containing one slice of the target area (human brain)
- volume: one sample of 3D dataset containing a lot of slices and making up the whole target (human brain)
- image/scan: one sample of dataset after one image reconstruction. They are quite similar, though regularly, scan means the product of MRI at an exact time point (scan time), while image is the visualization of a scan after some evaluation mostly in radiological convention (as on my Figures); which means the left hemisphere are situated on the right side while the right one on the left (as looking the laying patient from his feet).

Concept

Any MR experiment can be described as involving three consecutive events: equilibrium, excitation and relaxation.

For clinical imaging purpose, we record signals principally from the nuclei of hydrogen, consisting of a single proton. There are two main reason of it: there are a lot of them (mainly in water); and it is so called magnetically active as possessing net angular momentum (spin). With word "spins" we sometimes refer to magnetically active (i.e. MR-visible) nuclei. Spins placed in an external magnetic field with a magnetic vector B_0, will show precessing like little gyroscopes with a frequency of

$$\text{Eq.1.: } \omega = \gamma B_0$$

around the axis parallel with B_0. γ is called gyromagnetic ratio specific to a particular nucleus. In the equilibrium state, the magnetic field divides the water protons into two populations according to the orientation of the axis of their precessing. Some of the protons have axis parallel with B_0 (spin-up), whereas the others have an axis in antiparallel (spin-down) orientation. This division represents two distinct energy levels and results in a macroscopic magnetization due to the inequality of the populations. This energy level is proportional to B_0, as

$$\text{Eq.2.: } E = \hbar\omega = \hbar\gamma B_0.$$

During the excitation, if the energy absorbed is sufficient to equalize the populations of the two levels (see the Eq.2. – i.e. resonance), saturation occurs. A saturated system will return to equilibrium because of two simultaneous processes. First, the absorbed energy will be redistributed within the spin system by processes in which every transition of a spin from a higher to a lower level is accompanied by the transition of a spin from the lower to the higher state, called spin-spin relaxation. Second, there will be a gradual loss of energy to the other nuclei and the electrons in the material collectively called the lattice, resulting from transitions of excited spin from the upper to the lower state; this second process is called spin-lattice relaxation. The time constants characterizing these two processes are denoted by T_2 and T_1, respectively, i.e. the spin-spin (or transverse) and spin-lattice (or

longitudinal) relaxation times. Sometimes we are speaking about T_2*-relaxation time as characterizing a signal loss at a rate greater than T_2 caused by magnetic field distortions. In fact, the MR signal intensity, besides the spin density and diffusion, is determined by these physical properties and the sequence parameters.

In MR imaging (MRI) the signal of the sample is decomposed into spatial information, according to the frequency (resulting from applying a spatially varying magnetic field (gradient) additional to B_0) and the phase of the precession of the spins. In localized MR spectroscopy (MRS) besides the spatial determination of the signal, the individual resonances (as different nuclei possess different γ) can be determined to identify MR-visible metabolites.

1.2. Investigating brain structure and functions by means of MRI

1.2.1. Recording neural activities

1.2.1.1. Concept and Methods

Hemodynamical changes

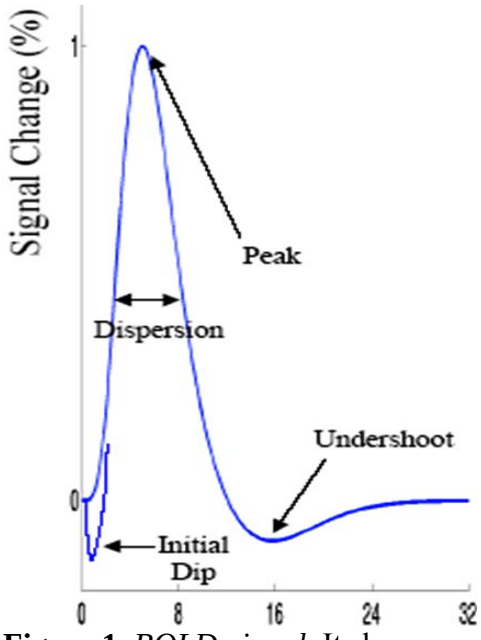

Figure 1. *BOLD-signal.* It shows a typical BOLD-response (with its properties) to an impulse stimulus.

Since the 1890s (Roy and Sherrington, 1896), it has been known that changes in blood flow and blood oxygenation in the brain (collectively known as hemodynamics) are closely linked to neural activity (neurovascular coupling), i.e. during brain activity, an increase in cerebral blood flow (CBF) can be observed. This finding also provides the base of positron emission tomography (PET). Almost one hundred years after Roy and Sherrington, Fox and coworkers

have found – beside the increased CBF – elevated cerebral metabolic rate (CMR) with elevated cerebral O_2-consumption, too. Roughly, neural activation is connected with de- and repolarization of membrane-potentials requiring energy so that increase in CMR. So, when nerve cells are active they consume more oxygen carried by hemoglobin in red blood cells from local capillaries. The response to this elevated oxygen utilization is a local increase in CBF, occurring after a delay of approximately 1-5 seconds. This hemodynamic response rises to a peak over 4-5 seconds, before falling back to baseline (after typically undershooting slightly) (Figure 1). Due to these local processes, there will be changes in the relative concentration of oxyhemoglobin and deoxyhemoglobin and changes in local cerebral blood volume in addition to change in local cerebral blood flow. Fox and coworkers showed that, the elevation of CMR was smaller than that of CBF (Fox et al, 1984; Fox and Raichle, 1986), resulting in a local decrease in the relative deoxyhemoglobin level.

BOLD-Imaging

Deoxyhemoglobin – with Fe^{2+} unshielded due to the absence of O_2 – is so called paramagnetic, i.e. it produces a small local magnetic gradient (magnetic susceptibility), i.e. distorting the magnetic field locally. This magnetic susceptibility enhances the T_2*-relaxation, resulting in decreased signal in T_2*-weighted images. In contrary, oxyhemoglobin is shielded with O_2, so it has no magnetic effect (non paramagnetic). Roughly, in an activated brain region the local decrease in the relative level of the paramagnetic deoxyhemoglobin causes decreased magnetic susceptibility leading to slower T_2*-relaxation, causing elevated signal in T_2*-weighted images, which can be detected using an MRI scanner. This technique is called blood oxygenation level dependent (BOLD) imaging, because recorded local signal intensity depends on the local level of O_2

(or rather local relative level of deoxyhemoglobin). It was found by Ogawa (Ogawa et al, 1990; Ogawa et al, 1992), and collectively called as BOLD-signal (Figure 1).

Paradigms

As this signal intensity variation is small (1-5% in general), many repetitions of activation (and scanning) and different statistical approaches are needed to determine the areas of the brain which reliably have more of this difference, so proved to be active during a task.

For example, if we want to determine, which brain area(s) is/are responsible for word generation, we should set up a schedule with many repetition of the task of word generation. This schedule is known as paradigm. It tells us the exact timing of the given task, so we are able to define – with the help of scan time – which scan was acquired in which phase of activation (Figure 2).

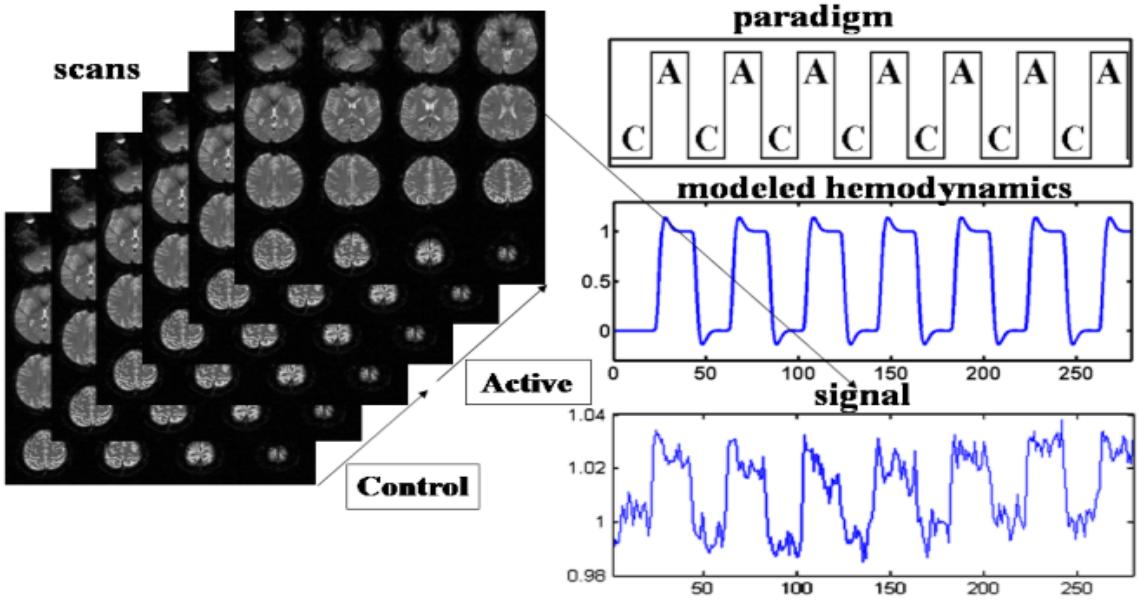

Figure 2. *Design of a functional measurement.* It demonstrates a paradigm for visualizing brain areas during word generation: During consecutive scanning (scans) and switching between the active (A) and control (C) phases, the T_2*-weighted signal intensity alters according to the paradigm, and it is similar to the expected one (modeled hemodynamics) derived from the paradigm.

Modeled hemodynamical changes

The easiest way of determining whether a voxel shows activation or not, would be a simple

subtraction or statistical comparison of the signal intensity in active and control phases. However, BOLD-response signal is not so simple (see Figure 1 and Figure 2), and the best fitting model of it is a set of Gamma Density-functions (called also as Basis Function). Moreover, in most of the cases stimuli are not impulses but take a longer period, which makes the problem more complex. With convoluting the paradigm with the Basis Function mentioned above, however, the whole hemodynamics can be adequately modeled (Figure 3 and Figure 2) resulting in a Hemodynamical Response Function (HRF).

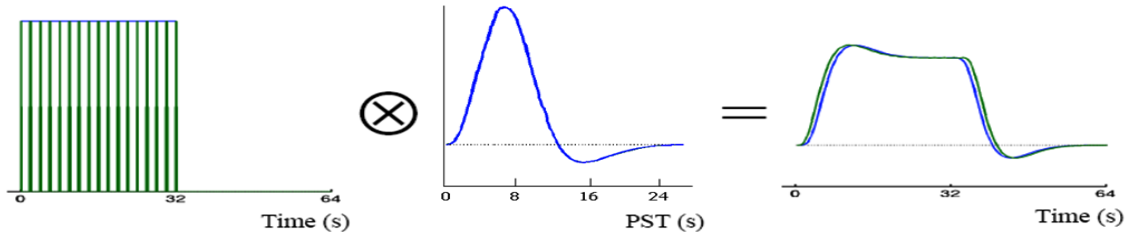

Figure 3. *Hemodynamical Response Function.* It shows how to model hemodynamics deriving from a paradigm with the help of the Basis Function. (PST: Post Stimulus Time)

Preprocessing

Usually the format and/or layout of the scans are not appropriate for analysis as they come out of the scanner; and therefore conversion, motion-correction and/or other transformation(s) are needed. These steps are collectively called preprocessing, as they take place before the analysis. There are a lot of them based on different approaches, but I will sum up just the most frequently used ones.

Motion correction is mostly used to reduce the effect of motion to the analysis. We should remind that the acquired space (field of vew – FOV) or voxels are defined referred to the scanner, which will measure always the same spots regardless of their content. One of the most disturbing cases is when motion correlates with the paradigm; e.g. during sequential finger opposition, the head of the subject is also moves due to the lack of stable fixation. In this case, around the edges or transitions from one tissue to the other voxel-content moves in and out of the measured space resulting a signal alteration correlating well with the

paradigm. In the end it will result in "activation". Motion correction – after calculating the rate of motion – simply "moves" the signal intensity back to its original position.

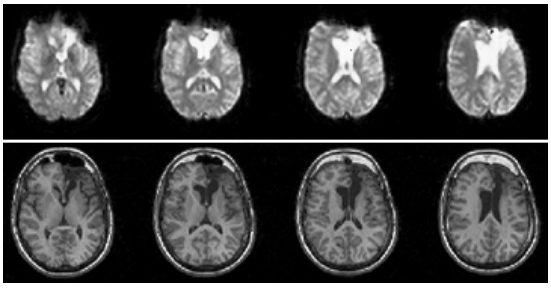

Figure 4. Example for coregistration.
Upper part: T_2*-weighted (fMRI)
Lower part: T_1-weighted (anatomical)

Coregistration (Figure 4) is very similar to motion correction, but works also between modalities; i.e. with its help we can transform a volume to a space of an other, even if it was acquired with different weighting.

As everyone's brain has its own shape, when we want to compare the images from more subjects (e.g. in a group-analysis) we have to transform them into a common – so called standard – space. This process is called normalization. In this standard space – according to either the Talairach- (Talairach and Tournoux, Stuttgart 1988) or the MNI- (Collins, 1994) atlas –, every brain structure has its own place; therefore volumes transformed into standard place will contain the structures on the same spot. So they can be easily analyzed and – as these coordinates are worldwide used and accepted – referring to them we speak about the same structure everywhere in the world.

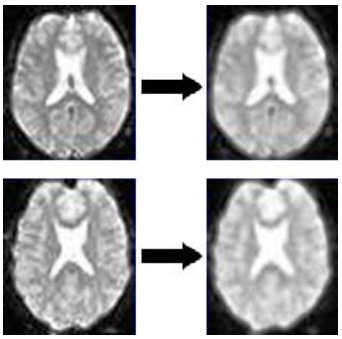

Figure 5. Smoothing images of two subjects.

Smoothing (Figure 5) applies a 3D Gaussian filter onto the volume convoluting the signal intensities with it. As a result, it increases signal-to-noise ratio, decreases anatomical intersubject variability at the cost of lowering spatial resolution and increasing partial volume effect i.e. making localization less accurate. Unfortunately, there is no generally accepted rule or objective measure for temporal or spatial smoothing in fMRI, though its effect was already investigated (Scouten, Papademetris and Constable, 2006). In any case, smoothing interferes with a number of image features that may affect a

subsequent data analysis such as used in fMRI. As a rule of thumb, smoothing – in fMRI – should be used basically only for the group analysis to reduce the anatomical intersubject variability additionally increased by imperfect spatial normalization.

Statistical evaluation

The aim of evaluating fMRI dataset is to classify the voxels as active, deactive or none. To do this, statistical approaches are used to examine and quantify the similarity of signal intensity alterations to the HRF (Figure 2).

There are many approaches available but the General Linear Model (GLM) is the most widely used. The popularity of it is due to its linearity, which makes it theoretically and computationally tractable. In the framework of the GLM – similarly to the equation of a line:

Eq.3.: $Y = bX+a$

–, it is possible to describe a BOLD-response with a linear combination of explanatory variables and residual variability (Figure 6).

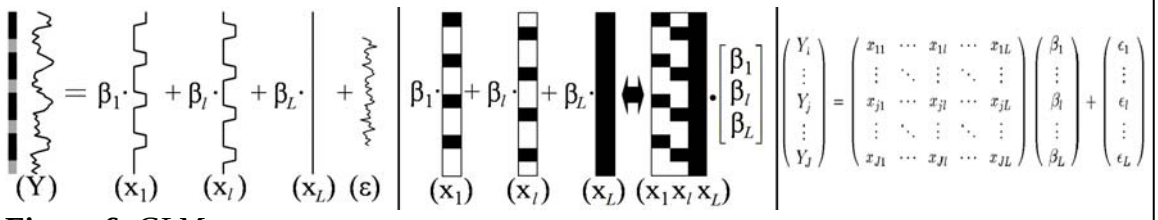

Figure 6. *GLM*.
Left part: Representation of the signal and HRF.
Middle part: Graphical representation (as can be seen in most softwares).
Right part: Mathematical representation (as it is evaluated).

In the equation of GLM ($Y = \beta X+\varepsilon$), Y represents our signal change, as being the independent variable; set of β-s represents the linear combination (known also as parameter values), acting like weightings of the explanatory variables represented by X and known also as covariates or regressors. ε stands for the residual variability (known also as error). It comes from the physiological a technical noise so it is independent from our measurement

and has a normal distribution. During estimation, by means of linear regression we try to find the parameter values, with that the linear combination best fits the data. In the end, applying different statistics (t- or f-test), we can calculate which voxels are affected significantly by our paradigm; as these voxels will have shown a significantly high β-value belonging to the given paradigm. These voxels will be called “activated”.

Setting threshold(s)

In the end, similarly to any other statistics, we have to declare level of significance or threshold. And also as a statistical method, it may produce false positive and negative results. Because of the great number of estimation (at a common spatial resolution of $3x3x3mm^3$, we have about 50000 voxels), risk of false positives is much higher; therefore a simple threshold would surely give false result.

Apart from different correction methods coming from statistics, such as controlling False Discovery Rate (FDR) (Genovese, Lazar and Nichols, 2002) or FamilyWise Error (FWE) rate (Nichols and Hayasaka, 2003), there are approaches taking account physiological properties of neurovascular coupling.

The most widespread method is, besides setting a threshold on a statistical basis, applying a second threshold on the basis of number of concurrently activated neighboring voxels (aka cluster extent). It can also be used in Statistical Parametric Mapping (SPM) (Friston et al, 1995), which is the most commonly used software for analyzing functional datasets. A potential drawback of this method is that it requires subjective thresholding. Generally, as the statistical threshold decreases, the volume of "true" activation increases (as more and more voxels survive it), but at some point we will see a lot of "scattershot" (false positive) clusters throughout the brain. At that point we should back off to use a more stringent criterion. When preparing results e.g. for a neurosurgical intervention, we can try to

maximize the area of activation with minimal false positives in the vicinity of the area of intervention. Visualizing the activation across multiple planes sometimes clarifies whether scattered activation along the fringes of a tumor is part of a larger cluster. Moreover at lower threshold we can "eliminate" the small clusters simply with increasing the extent threshold. Sometimes, however, at lower statistical threshold these small (false positive) clusters build up for a bigger one hard to eliminate.

On the other hand a fMRI data processing method has been established (Baudewig et al, 2003) that emerges as a rather simple data-driven approach originally motivated by detailed experimental observations and physiologic considerations (Kleinschmidt et al, 1995). The method is referred to as Two-Threshold Correlation (TTC) and has evolved during the analysis of several thousands of fMRI data sets acquired in multiple studies of the Göttingen laboratory. It is based on cross-correlation, which – like linear regression – examine similarity of signal intensity changes to HRF, and characterize it with correlation coefficient (CC). The CC maps are thresholded individually by estimating the noise distribution underlying the distribution (or histogram) of correlation coefficients of the *actual* fMRI acquisition. In fact, studies without any stimulation (Null experiment) demonstrated that the width of a corresponding CC distribution may be affected by alterations of the hemodynamic responsiveness (`arousal'), respiration, perfusion, flow-induced tissue pulsations, or motions. Because the basic form of these distributions is adequately described by a Gaussian curve, true brain activations, that is voxels representing paradigm-associated fMRI signal alterations, may be easily identified: the CC histogram of a fMRI study emerges as the sum of a dominating noise distribution and a second much smaller distribution of activated voxels with high positive (or negative) CC values. In contrast to methods based on a single threshold, the TTC method employs two probabilistic thresholds for their separation: a high value for the identification of highly

significant activations and a lower value for limiting the iterative addition of directly neighboring voxels to these centers. The approach ensures both specificity and sensitivity for defining the spatial extent of significant activation spots. So, if – similarly to the example above – we want to maximize the area of activation in the vicinity of the area of intervention, just decreasing the lower threshold will not result in "scattershot" (false positive) clusters throughout the brain.

1.2.1.2. Group analysis

Functional magnetic resonance imaging of human brain activation is a non-invasive method for monitoring hemodynamic responses to a functional challenge in single subjects with high spatial and temporal resolution. However, in view of increasingly complex cognitive paradigms that often involve only subtle differences in neural activity, the response strengths tend to decrease and impose severe challenges for adequate post processing. In addition, in longitudinal or cross-sectional studies, we are usually looking for activation characterizing a group of subjects. A common strategy is therefore to move from single subject to group analysis, which is also incorporated into SPM. Though elegantly designed for the statistically trained and experienced researcher, a potential drawback of the method is its complexity even at single subject level. As a consequence, SPM applications require substantial knowledge with the potential risk that the rank-and-file user may be misguided to produce inadequate results.

On the other hand TTC has already been published, that circumvents the not only the problem of false positive activation but also the inconvenience of subjective thresholding (see above). Nevertheless, the great advantages of TTC could have utilized only at single subject level.

1.2.1.3. FMRI in neurosurgical evaluation

Cortical (re)organization of cerebral functions

Neurosurgical diseases often serve as a "model disorder" for many functional neuroimaging methods because in some localization-related cases the pathogenic area should be surgically removed. Apart from saving the patient's life, we also try to preserve brain regions which contribute significantly to normal brain process. This is true even more in epilepsy surgery as not a life-saving operation. The "insignificant" contribution can be resulted due to representation of certain brain processes in a network; and one region removed from this network will be compensate by the other network elements (for example in the case of functions with bilateral representations the region contralateral to the resection can also represent the functions of the removed structure). Moreover, the "insignificant" contribution is that some brain functions can be quickly reorganize after brain surgery. Finally, the functions of e.g an epileptogenic focus can also reorganize and shift to healthy brain areas even before the operation due to the presence of structural lesion or due to chronic functional disturbance caused by frequent seizures or interictal epileptic activity (Janszky et al, 2003a; Janszky et al, 2003b). Brain regions thought to be contributed significantly in the healthy brain functions without compensatory reorganization capacity are called eloquent areas. One of the challenges in neurosurgical evaluation is to differentiate eloquent areas from the other brain tissue and to determine their relationship to the area of intervention. This work-up may require the whole arsenal of functional investigations including Video-EEG, neuropsychological tests, fMRI, SPECT, PET, functional TCD, Wada tests or even using pre- or intraoperative intracranial electrode stimulation in order to asses of the functional properties of an epileptic focus. Thus, any new methods investigating brain functions were first validated by invasive or well-known tools using in neurosurgery. Numerous studies demonstrated reliability and

reproducibility of fMRI examinations, which resulted in a wide distribution of fMRI methods in neurosurgical evaluation.

One of the most frequent neurosurgical interventions is the operation of temporal lobe epilepsy (TLE). The epileptogenic region of the TLE is usually localized in the medial temporal structures, their removal is superior to drug therapy in curing TLE (Wiebe, Blume and Girvin, 2001) and lead to complete cessation of seizures in 60-90% (Janszky et al, 2001; Janszky et al, 2005a). Consequently, the resection of these structures – anterior partial temporal lobectomy or selective amygdalo-hippocampectomy – is the most frequently used surgical procedure in intractable TLE (Janszky et al, 2001). Conversely, the possible side-effect of the mesiotemporal resections may be memory impairment, because the mesiotemporal structures play a crucial role in memory functions. Although the neurpsychological tests and the presence of structural damage of the mesiotemporal structures predict the postoperative memory loss in some degree, the intracarotid amobarbytal (Wada) test is the "gold standard" for testing the memory functions of the mesiotemporal structures and for predicting the postoperative memory problems. In the past five years, there were some studies using fMRI in visualizing the memory functions of the mesiotemporal structures, showing that, the non-invasive fMRI investigating memory functions may replace the Wada test (Jokeit, Okujava and Woerman, 2001). By using fMRI, more patients can more easily investigated than in Wada test and the results can be compared with normal subjects due to its non-invasive nature. Preliminary data suggest that memory fMRI can predict the postoperative memory decline in TLE by determining whether a reorganization of memory functions took place and the representation of memory shifted to the structures contralateral to the epileptic focus (Janszky et al, 2005b).

In almost all cases of neurosurgical interventions, to avoid postsurgical speech distubances, language lateralization has to be known prior to epilepsy surgery. FMRI can be used in the

majority of patients otherwise undergoing the Wada test, because speech-activated fMRI acquisition and assessment have become easy and reproducible, and fMRI provides typical (left-sided speech) and atypical (right-sided speech) results in large numbers of individual cases in concordance with Wada test, though, the risk of falsely categorizing language dominance using fMRI seemed to be particularly high in extratemporal localization-related epilepsy (Woerman et al, 2003).

Besides areas concerning memory and language, other eloquent brain areas such as visual system (Belliveau et al, 1991) and senso-motor system (Kim et al, 1993) can also be routinely visualized by fMRI, which makes the neurosurgical evaluation and determining the extent of resection more easily.

Studying pathomechanism of human epilepsy by fMRI

The fMRI combined with simultaneous EEG (EEG-fMRI) is a new technique, which was developed in the last few years. It combines the advantages of EEG (specificity to functional abnormalities underlying epilepsy and high temporal resolution) with the advantages of fMRI (high spatial resolution). At present, this technique can demonstrate epileptic functional disturbance with the highest spatial and temporal resolution providing a unique opportunity to study the pathophysiology of epilepsy in humans (Krakow et al, 1999; Gotman et al, 2005). Although the technique is not available or not used in most neurosurgical centers, in the future it can be one of the major tool in identifying pathological electrophysiological event in epilepsy and their site of origin ("spike mapping"). Moreover, it is a novel method in investigating sleep and its disorders.

However, it has its own limitations. Scalp EEG detects electric potential fields some distance from the source, resulting in very low spatial resolution. The invasive intracranial EEG can only measure electrical changes during epileptic seizures that are in the vicinity

of the electrodes. Because the whole brain cannot be implanted by electrodes, a sampling error must always occur during intracranial recordings, thus neuronal activity distant from the electrodes remains undetected (Siegel et al, 2000). Using ictal SPECT or PET, epileptic activity can only be visualized at the time of the tracer binding (Koepp et al, 1998), thus it often visualizes seizure spread but not seizure onset (Janszky et al, 2002). Magnetoencephalography (MEG) can exclusively detect an overall electromagnetic brain activity but with low spatial resolution (Knowlton and Shih 2004).

It is well known that regional increases in brain perfusion coincide with ictal activation (Penfield et al, 1939). In addition, epileptic seizures are accompanied by abnormally large neuronal activity (Engel et al, 2007, Uhlhass and Singer, 2006). Functional magnetic resonance imaging (fMRI) can provide maps of human brain functions with acceptable temporal and high spatial resolution and, theoretically, this abnormally large activity can be produce hemodynamical changes much better detected with FMRI in comparison with normal neuronal processes. Consequently, spatiotemporal visualization of epileptic activity can be the first step in developing methods to demonstrate whole-brain neuronal activity in general, with adequate resolution in time and space. However, until now, no technique has been able to adequately visualize the spatiotemporal relationship of the spreading activity during epileptic seizures. Hence, there is a growing literature concerning the detection of blood oxygen-dependent (BOLD) signal changes during epileptic seizures, including clinical and subclinical ictus (Jackson et al, 1994; Detre et al, 1995; Detre et al, 1996; Kubota et al, 2000; Krings et al, 2000; Federico et al, 2005; Salek-Haddadi et al, 2002; Kobayashi et al, 2006; Salek-Haddadi et al, 2006). Further, haemodynamic pattern changes over time can refer to the spread of the epileptic activation (Hollo et al, 2001; Janszky et al, 2002). Visualization of epileptic activity in the brain with good spatial resolution is of critical importance for the neurosurgical evaluation of epileptic patients; however, there is

no study in the literature that successfully demonstrated whole-brain, spatiotemporal, haemodynamic changes during a clinical seizure.

1.2.1.4. Combining with DTI-FT (function and structure)

FMRI allows for a noninvasive visualization of functioning brain areas, but has limited info about connections and white mater. The absence of activation – e.g. after traumatic brain injury (TBI) – can be caused by either the damage of the brain area or the damage of the connection to that area. If we want to determine the severity and the likelihood of possible outcomes, the information about connections is also necessary.

Diffusion tensor imaging (DTI) can measure anatomical connectivity between areas with MR. Although it is not strictly a functional imaging technique because it does not measure dynamic changes in brain, the measures of inter-area connectivity it provides are complementary to images of function provided by BOLD fMRI.

The basic principles of 'plain' diffusion MRI were laid out in the mid 1980s (see for instance Le Bihan, 1995 for a review).With its help tissue structure can be examined at a microscopic level well beyond the usual MRI resolution. During typical diffusion times of about 50-100 ms, water molecules move in the brain on average over distances around 10-15 μm, bouncing into, crossing or interacting with many tissue components, such as cell membranes, fibers or macromolecules. In more pathology, changes in the diffusion can be observed in a very early phase; proved to be extremely useful in routine diagnostics. The most successful application of diffusion MRI since the early 1990s has been acute brain ischemia (Albers et al, 2000; Baird and Warach, 1998).

Furthermore, as diffusion is truly a three-dimensional process, molecular mobility in tissues is not necessarily the same in all directions, as it was already detected for the first time in vivo at the end of the 1980s in white matter (Moseley, Cohen and Kucharczky,

1990; Chenevert, Brunberg and Pipe, 1990). This diffusion anisotropy may result from the presence of obstacles, especially the ones with directionality (e.g. bundles of more or less myelinated axonal fibers), that limit molecular movement differently in each directions. It was quickly apparent that this feature could be exploited to map out the orientation in space of the white matter tracks in the brain, assuming that the direction of the fastest diffusion would indicate the overall orientation of the fibers (Douek et al, 1991). Work on diffusion anisotropy really took off with the introduction in the field of diffusion MRI of the more rigorous formalism of the diffusion tensor (DT), by Basser and coworkers (Basser, Mattiello and Le Bihan, 1994; Basser and Jones, 2002). With the formalism of tensor, a property – in this case, diffusion anisotropy effects – can be extracted, characterized and exploited along more axis of a coordinate system – in this case, the space – providing even more exquisite details of tissue microstructure. Many studies have been published thereafter dealing with the optimization of the MRI sequences necessary to get access to the diffusion tensor, the processing and the display of DTI data (Pierpaoli and Basser, 1996; Pajevic and Pierpaoli, 1999), and of course, potential applications. After evaluating DT-data, fractional anisotropy (FA) describing the diffusion profile of the water can be obtained. FA can have a value between 0 (perfectly isotropic – spherical profile – diffusion) and 1 (infinitely anisotropic – infinitely elongated profile – diffusion).

The most advanced application is certainly that of fiber tracking (FT) in the brain (reviewed by Mori et al, 2002), which can visualize the neural tracts with tracking the DT. This technique is able to detect damage of the tracts and other alterations, such as TBI (Huisman et al, 2004), brain tumor (Yu et al, 2005) or multiple sclerosis (Hesseltine et al, 2006); or even pathological connectivity in dyslexia (Duetsch et al, 2005) or schizophrenia (Schlosser et al, 2007). In combination with fMRI, it might open a window on the important issue of functional networks (Le Bihan and van Zijl, 2002).

1.3. Low magnetic field

Functional magnetic resonance imaging (MRI) allows for a noninvasive visualization of activation in human brain that are engaged in information processing in relation to the performance of a specific task or the perception of an external (or internal) stimulus. Accordingly, such methods may prove invaluable for the diagnosis of functional deficits in a wide variety of patients with brain disorders. Because the MRI-detectable hemodynamic response to a change in neural activity depends on the microscopic magnetic susceptibility changes that are induced by changes in the absolute concentration of deoxyhemoglobin, its sensitivity is commonly expected to increase with the strength of the static magnetic field. So far, only a limited number of low-field functional MRI studies have been reported in the literature (Jones et al, 1998; Van Borsel et al, 2003; Lundervoldt et al, 1995; Santosh Rimmington and Best, 1995; Hoogenraad et al, 1998). In fact, all comparative studies using echo-planar imaging (EPI) at a high and low field (Gati et al, 1997; Turner et al, 1993; Krasnow et al, 2003; Fera et al, 2004; Krüger, Kastrup and Glover, 2001) indicated that a higher field strength is unquestionably superior, so that the authors of a successful functional MRI study at 1 T felt tempted to disqualify their own results as "somewhat controversial" (Jones et al, 1998). However, the increased sensitivity to macroscopic susceptibility artifacts at higher fields is certainly disadvantageous for many clinical conditions. For instance, hippocampal activations in response to a mental navigation paradigm used in epilepsy (Janszky et al, 2004) are often hampered by pronounced EPI signal losses and geometric distortions in the vicinity of air-filled cavities and sinuses (Gati et al, 1997; Merboldt et al, 2001). Furthermore, neurosurgical patients who underwent a preceding brain operation may have defects in skull bone which also result in severe susceptibility artifacts compromising EPI of residual neighboring tissue – the obvious target of functional MRI studies in these cases.

In our country, most of the MR-scanners are operating at lower field (maximum 1.5Tesla), known to have lesser sensitivity and worse signal-to-noise ratio (SNR). Moreover, producers of scanners are also urging to buy newer, more modern machines capable of novel techniques. However, thanks to the technical developments, with modern scanners operating at low field better homogeneity and formidable sensitivity in detection can be achieved. Therefore, methods having required higher field earlier (such as fMRI) can now be conducted at low field, too; even with intraoperative scanners usually operating at lower than 1.5T.

With proper settings of acquisition parameters and appropriate post-processing methods sensitive enough to detect activation at low field, possibility of applying novel imaging techniques becomes in reach of wider community: It would extend the diagnostic possibilities for a wide spectrum of neurological/neurosurgical patients, would enable us to utilize low-field (and usually cheaper) scanners for screening; and would provide its useful methods for neuroscientists. For all, who have access only to low-field MRI systems.

1.4. Comparing fMRI with other functional imaging techniques

Positron Emission Tomography (PET)

PET measures emissions from radioactively labeled metabolically active chemicals that have been injected into the bloodstream and had produced by a cyclotron. The labeled compound, called a radiotracer, is injected into the bloodstream and eventually makes its way to the brain. Sensors in the PET scanner detect the radioactivity as the compound accumulates in various regions of the brain. Especially useful are a wide array of ligands used to map different aspects of neurotransmitter activity. The most commonly used PET tracer is, however, a labeled form of glucose (2-fluoro-2-deoxy-D-glucose (FDG)) because of its price.

The greatest benefit of PET scanning is that different compounds can show blood flow and oxygen and glucose metabolism in the tissues of the working brain. PET scans were superior to all other metabolic imaging methods in terms of sensitivity and speed of completion (as little as 30 seconds), when they first became available. The biggest drawback of PET scanning – apart from its invasivity and high price – is that because the radioactivity decays rapidly, it is limited to monitoring short tasks.

Single Photon Emission Computed Tomography (SPECT)

SPECT is similar to PET and uses gamma ray emitting radioisotopes and a gamma camera to record data. SPECT relies on an injection of radioactive tracer, which is rapidly taken up by the brain but does not redistribute. Uptake of SPECT agent is nearly 100% complete within 30 - 60s, reflecting cerebral blood flow (CBF) at the time of injection. In contrast to PET, SPECT is able to make use of tracers with much longer half-lives, such as technetium-99m, and as a result, is far more widely available. Thanks to the longer half-live, it is particularly well suited for detecting longer events, such as epileptic seizures, because scans can be acquired after seizure termination (so long as the radioactive tracer was injected at the time of the seizure). A significant limitation of SPECT is its poor resolution (more cm) compared to that of fMRI.

FMRI

FMRI can detect brain activity without any radioactive agent. To our present knowledge it is completely noninvasive, making fMRI usable several times in case of monitoring, screening or conducting a complex cognitive study. Its superiority in spatial resolution and availability (in terms of both presence and price) are also unquestionable.

In other hand, due to its low sensitivity, more repetitions of a task are needed, which limits

its usability. Single or rare events with longer duration – such as seizures and other 'ictal' events – are hard or impossible to detect with fMRI. The other main limitation is that not everyone can be put into scanner: e.g. epilepsy patient with large movement, small children, subject with pacemaker or tattoo; or even with enlarged abdominal circumference caused by overweight. This latter is a growing problem in e.g. United States.

Although, there is no one-for-all procedure, and sometimes we have no choice but to use the only one suitable; there is a trend to move towards fMRI, because – regarding to all aspects – fMRI is the best candidate for routine diagnostic purpose and neuroscientific research as well.

Table 1. Comparison of functional imaging techniques

	fMRI	**SPECT**	**PET**
Sensitivity	low	good	exceptional
Spatial resolution	millimeters or below	centimeters	centimeters
Temporal resolution	seconds or below	minutes	minutes
Tasks – Duration	< 1 minute	minutes	< 1 minute
Tasks – Complexity	simple or complex	simple	simple
Examination time	5-15 minutes	15 minutes	minutes
Invasivity	stationary magnetic field (whole body) radiofrequency (~100 MHz) (local) magnetic gradients (local)	radioactivity (whole body)	radioactivity (whole body)
Price (examination)	x 10.000 HUF	> 100.000 HUF	x 100.000 HUF (+cyclotron!)
Availability in Hungary	more per county (1T)	more per county	3-5/country

1.5. Aims

- (i) to optimize both image acquisition parameters and post-processing appropriate for reliable low-field functional MRI studies and (ii) to assess its reliability in comparison to acquisitions at 3T

- to demonstrate its feasibility in routine diagnostics: both in preoperative neurosurgical evaluation and intraoperative functional neuronavigation, as well as postoperative control

- (i) to develop a new approach in group analysis of fMRI data with all the advantages of TTC and (ii) to prove its reliability comparing its results to corresponding group analyses with SPM

- by means of ictal-FMRI during an epeileptic seizure at low magnetic field, (i) to highlight the site of the initial haemodynamic alteration (i.e. putative seizure-onset zone) and (ii) to visualize haemodynamic changes associated with seizure propagation

- to determine the level of the functional and structural damage in the algorithm of work-up of a patient suffering from severe traumatic brain injury (TBI) with combining fMRI with DTI both performed at low magnetic field, and comparing the DTI-results with that of a healthy subject

- to visualize brain activity during Déjà Vu (DV) by applying suitable functional neuroimaging (SPECT)

2. Materials and Methods

2.1. Recording neural activities by means of MRI at low magnetic field

2.1.1. Optimizing parameters at low magnetic field

2.1.1.1. Basic paradigms and clinical application

Subjects and paradigms

Basic examinations were carried out on normal adults. During continuous EPI-acquisition block designs with alternating active and control periods were applied. Ten-ten images were acquired during both the active and the control periods; and the two images acquired during the intermediate phase (i.e. in the beginning of the periods) were excluded from the analysis. With six cycles of control and active periods, the whole examination – one paradigm – lasted about four minutes. The following tasks were applied:

(a) sequential finger-to-thumb opposition (SFO) and motor rest (Baraldi et al, 1999) at the speed of 1-2 Hz, suitable to visualize brain activity in gyrus prae- and postcentralis

(b) internal word generation (IWG) (generating words beginning with a given letter without pronunciation) and rest (Woerman et al, 2003), suitable to visualize brain activity in speech centres (Broca's and Wernice's areas)

(c) mental navigation using visuospatial memory (Jokeit, Okujava and Woerman, 2001), suitable to visualize brain activity in hippocampal formation. The task is to navigate – in mind – from one place to an other (e.g. from home to work), recalling the most scenes known by the subject.

MRI

Low-field MRI examinations were conducted on a clinical system operating at 1T (Siemens Magnetom Harmony, Erlangen, Germany). A standard Siemens circularly

polarized head coil was used for signal excitation and detection. Functional studies employed an EPI sequence as supplied by the manufacturer with the following parameters: TR/TE = 2000 ms/80 ms, $\alpha = 90°$, BW = 752 Hz, FOV = 200 × 200 mm and matrix 64 × 64 yielding 3.1 × 3.1 mm in-plane resolution, and 16 sections with a thickness of 5 mm and 1 mm gap.

Data processing

A retrospective motion correction and data analysis was performed using Syngo-software as offered by the manufacturer. Voxels showing signal intensity significantly higher in active than in control period were determined with t-test. After z-transform, a threshold of $z > 3.5$ was applied in all cases providing a level of significance $p = 0.0002$.

2.1.1.2. Comparative study at 1T and 3T

Subjects and Paradigms

Eight healthy normal volunteers (male, right-handed, mean age: 31±4 years) participated in the study. Handedness was examined by the Edinburgh Inventory Test (Oldfield, 1971). Approval by the Institutional Review Board was obtained and all subjects gave written informed consent before each examination.

Mapping of eloquent language and sensorimotor areas was accomplished with use of a block design alternating active and passive periods each lasting for 50 s. The paradigms involved (i) 7 cycles of internal word generation (IWG) (generating words beginning with a given letter) and rest (Woerman et al, 2003), (ii) 5 cycles of sequential finger-to-thumb opposition (SFO) and motor rest (Baraldi et al, 1999), and (iii) 5 cycles of a passive finger movement (PFM) (investigator moved the fingers of the volunteer according ref. (Holloway et al, 2000)) and motor rest. During SFO the subjects' cooperation was visually

monitored and for passive movements a similar frequency of 1-2 Hz was chosen. Subsequent to a word generation paradigm subjects were interrogated with respect to their performance.

MRI

Low-field MRI examinations were conducted on a clinical system operating at 1T (Siemens Magnetom Harmony, Erlangen, Germany). A standard Siemens circularly polarized head coil was used for signal excitation and detection. Functional studies employed an EPI sequence as supplied by the manufacturer with the following parameters: TR/TE = 2500 ms/80 ms, $\alpha = 90°$, BW = 752 Hz, FOV = 192 × 192 mm and matrix 64 × 64 yielding 3 × 3 mm in-plane resolution, and 16 sections with a thickness of 3 mm and 1 mm gap.

Corresponding high-field MRI examinations were conducted at 3T (Siemens Trio, Erlangen, Germany). Excitation was performed with the body coil, while signal reception was achieved with an 8-channel head coil. Again, a standard EPI sequence was applied with the following parameters: TR/TE = 2500 ms/36 ms, flip angle 80°, receiver bandwidth 1184 Hz, and 20 sections. Other parameters were identical to those used at 1 T.

Data processing

At both field strengths a retrospective motion correction was performed as offered by the manufacturer. Significant activations were identified by two different statistical evaluations using either a single-threshold *t*-test (SPM) or a two-threshold correlation analysis (TTC). In the first approach, a single-subject and group analysis of all 1 T and 3 T data were performed with SPM5 (Friston et al, 1995) applying a low statistical threshold of $p = 0.05$ (family-wise error (FWE) corrected (Nichols and Hayasaka, 2003)). Concurrent activation

of a cluster of at least 10 neighboring voxels was assumed to represent a true spot of activation and a 6s long delay in haemodynamic response was applied similar to TTC analysis. Only in the group analysis, the images were normalized to the standard MNI space (Collins, 1994) and subjected to a spatial Gaussian filter of 5 mm full width at half maximum.

Alternatively, all data sets were evaluated on a single-subject basis using a two-threshold correlation (TTC) analysis (Kleinschmidt et al, 1995; Baudewig et al, 2003) (see abowe). In comparison to SPM, the method is rather data-driven and does not require subjective thresholding either in the *t* score or the number of concurrently activated neighboring pixels. A particular strength of the method is the ability to account for intertrial variability in the noise distribution that may be caused by residual motions or systemic physiologic changes unrelated to the task (Kleinschmidt et al, 1995). Further, the TTC method minimizes the problem of false positive activations because any accepted activation is based on a central spot (i.e., at least one pixel) with a correlation coefficient that corresponds to a $p = 0.0001$. The lower threshold of 0.05 only applies to the outer boundary of such highly significant centers.

Region of interest analyses of activation volumes (i.e. number of activated pixels) and MRI signal intensity time courses were performed in the Broca and sensorimotor cortex in all subjects and examinations individually, based on the TTC- and single-subject SPM-results. The locations of these regions were identified by an overlay of respective Brodmann areas using freeware software (MRIcro) in each examined MRI section. In the target regions, the analysis was based on the largest activation cluster including neighboring slices.

Statistical Analysis

Data processing and statistical analysis was performed with MatLab 6.5 software. One-tailed, paired *t*-test was applied to identify significant differences (i.e., $p = 0.05$) in the number of activated voxels. The signal-to-noise ratio (SNR) of the images was determined by dividing the mean of all intensities originating from the brain by the standard deviation of all intensities outside the head (i.e., air).

2.1.2. Diagnostic studies (neurosurgical planning and functional neuronavigation)

Patients and paradigm

From 2005 October to 2007 October, in 48 patients (female: 24, male: 24; age (mean and range): 40 (10-68)), preoperative fMRI was accomplished to determine the exact location of eloquent area, due to the location of intervention near to them.

Most of them suffered from recurrent headache; however, there were 10 case of epilepsy as a main indication, too. Neuroimaging resulted in mostly glioma from grade I-III; though, there were also several cases of meningeoma, cavernoma and dysgenesis.

Altogether, 114 fMRI sessions were conducted:

- 50 session of internal word generation (IWG) (see above)
- 22 session of story listening involving 7 cycles of story listening and rest (listening to the background (i.e. scanner) noise)
- 21 sessions of sequential finger-to-thumb opposition (SFO) (see above): 14 on the right, 6 on the left, 1 on both sides
- 20 sessions of passive finger movement (PFM) (see above): 11 on the right, 9 on the left side
- 1 session of feet movement involving 5 cycles of motor activity and rest

Mapping the eloquent areas was accomplished with use of the block design alternating

active and control periods. In the first 6 sessions (3 patients), each periods lasted for 25 s, then – to increase the sensitivity and SNR 50s-long periods were used. In one case of a 10-years-old boy, 37.5s-long periods were chosen to decrease the session time while maintaining the sensitivity.

MRI

Examinations were conducted on a clinical system operating at 1T (Siemens Magnetom Harmony, Erlangen, Germany). A standard Siemens circularly polarized head coil was used for signal excitation and detection. Functional studies employed an EPI sequence as supplied by the manufacturer with the following parameters: TR/TE = 2500 ms/80 ms, α = 90°, BW = 752 Hz, FOV = 192 × 192 mm and matrix 64 × 64 yielding 3 × 3 mm in-plane resolution, and 16 sections with 1 mm gap. In most of the cases a slice thickness of 3 mm was applied; however, in several cases – to increase sensitivity – 5 mm was chosen.

After the fMRI, T_1-weighted (anatomical) images used for intraoperative neuronavigation were acquired applying a 3D FLASH-sequence with the following parameters: TR/TE = 2110 ms/4.38 ms, α = 15°, BW = 130 Hz, voxel size 1.3 mm isotropic. In some cases, 10 ml Magnevist® (gadolinium) was also used as a contrast agent.

Data processing

A retrospective motion correction was performed as offered by the manufacturer. For the first 6 patients (22 sessions), significant activations were identified by using SPM5 (Friston et al, 1995). Statistical threshold was set to p = 0.0003 (uncorrected), resulting in T > 3.5; and concurrent activation of a cluster of at least 10 neighboring voxels (extent threshold) was assumed to represent a true spot of activation. To provide information more suitable for neurosurgical evaluation, activation map was overlaid onto the previously coregistered anatomical images with the help of CBMGtools (an extension for SPM5).

Later, TTC was applied to analyze datasets for diagnostic purpose. As it is discussed in 1.2.1.1. *Setting threshold(s)*, it is less user-dependent, easier to use for "one-click-and-go" evaluation; and ensures both specificity and sensitivity for defining both the location and the spatial extent of significant activation spots. The program was written by me under MatLab 6.5 software.

Preoperative neuropsychological examination

In a few cases, to determine whether the operation will have caused any neuropsychological alteration, in addition to the routine examinations, Hungarian version of the Addenbrooke cognitive examination (ACE) (Stachó et al, 2003) were conducted. Provided results could be used to compare pre- and postoperative mental abilities of the patient. ACE over 80% is accepted as normal. With all these neuropsychological tests we could assess the reliability of FMRI.

Operation

Surgery was conducted with the help of Medtronic Treon neuronavigation system with an accuracy of about 1.3 mm.

For navigation, the same images were used as the one used for overlaying the activation map. So, beside the location of the tumor, the location of the eloquent speech center was also visualized.

Functional neuronavigation

From 2006 October, we are able to superimpose the activation map on the anatomical scan used for neuronavigation and save the result in DICOM format, so it can be uploaded onto the Medtronic Treon neuronavigation system. Activated voxels were given a value that is

two times higher than the voxel with the highest value in the anatomical image. In this way, the image retains good contrast while the activations are clearly displayed. The surgeon could rely on both structural data (location of the lesion) and functional data (location of eloquent areas) during the operation; thus increasing the radicality to the required extent while ensuring the intactness of indispensable areas.

Control examinations

In many cases, two to four weeks postoperatively, besides the contrast-enhanced anatomical MRI, fMRI and – in a few cases – neuropsychological examinations were conducted to determine the possible disturbance in mental ability or speech recognition caused by the operation. To detect the possible latent deficit in speech recognition, specific Token-test (Lezak, 1997) was also applied.

2.1.3. A novel group analysis

Participants and paradigms

Eight healthy normal volunteers (male, right-handed, mean age: 31 ± 4 years) participated in the study. Handedness was examined by the Edinburgh Inventory Test (Oldfield, 1971). Approval by the Institutional Review Board was obtained and all subjects gave written informed consent before each examination.

Mapping of sensorimotor and language areas was accomplished with use of a block design alternating active and passive periods each lasting for 50 s. The paradigms involved 5 cycles of unilateral sequential finger-to-thumb opposition (SFO) (right hand, frequency 1-2 Hz) and motor rest (Baraldi et al, 1999) and 7 cycles of internal word generation (IWG) and rest (Woermann et al, 2003).

MRI

MRI was conducted at 3 T (Siemens Tim Trio, Erlangen, Germany). Excitation was performed with the body coil, while signal reception was achieved with an 8-channel head coil. Functional MRI involved a standard EPI sequence (TR/TE = 2500/36 ms, $\alpha = 80°$) with an isotropic spatial resolution of 3 mm (24 sections). Motion correction was performed as offered by the manufacturer. All images were normalized to MNI space (Collins, 1994) and subjected to a spatial Gaussian filter of 5 mm full width at half maximum (FWHM). Both SPM and TTC post-processing steps were applied to these normalized and spatially smoothed images using MatLab 6.5 software.

SPM group analysis

Group analyses were performed with SPM5 (Friston et al, 1995). We have specified our fixed-effect model based on default settings of SPM with the eight subjects together using first-level analysis: Basic hemodynamic response function: canonical hrf, high-pass filter: cutoff: 128 s, global calculation: mean voxel value, grand mean scaling: session specific, global normalization: none. AR(1) model was used to account for substantial autocorrelations in fMRI data. We used contrasts "1 1 1 1 1 1 1 1" for activation and "-1 -1 -1 -1 -1 -1 -1 -1" for deactivation for the eight subjects respectively. A statistical threshold of $p = 0.05$ with FWE correction (Nichols and Hayasaka, 2003) resulting in $t = 4.66$ for IWG and $t = 4.62$ for SFO tasks, respectively. Activation and deactivation are shown on the same maps derived from t score maps produced by SPM5 software.

TTC group analysis

Similar to the established single-subject TTC analysis (Kleinschmidt et al, 1995; Baudewig et al, 2003), correlation coefficient maps were calculated for each subject with use of a

simple boxcar reference function derived from the task protocol and shifted by 6 s to account for the delayed hemodynamic response (Bandettini et al, 1993). Two CC thresholds for the group analysis were determined by fitting a Gaussian function to the central portion of the group distribution of CC values from all subjects and sections (i.e., from all individual CC maps). This part of the CC distribution has low CC values that do not refer to stimulus-correlated events. It may therefore be regarded as a representation of the noise distribution underlying the CC distribution of the actual experiment (Kleinschmidt et al, 1995).

With use of the estimated noise distribution the actual CC distribution was rescaled into percentile ranks of the noise distribution. Thus, the upper threshold chosen in the TTC analysis corresponded to the CC that matches the 99.99% (p value = 0.0001) percentile rank of the noise distribution. Voxels exceeding this value became automatically accepted as activated – they form the highly significant activation centers. Directly neighboring voxels were iteratively added to improve the area delineation around an activation center as long as their CC values exceeded a lower threshold corresponding to the 95% (p value = 0.05) percentile rank of the noise distribution.

After establishment of the individual CC thresholds for all sections, a voxelwise determination of respective group CC maps was achieved in two different ways: by a selection of either the maximum CC value (MAX) from the range of CC values of the individual CC maps or by calculating a mean CC value (MEAN) for each individual voxel. The resulting group CC maps were then analyzed with the previously determined thresholds in the prescribed manner to yield a group activation map for each section – similar to the procedure for a single-subject TTC analysis. Activations and deactivations were visualized on the same map. In order to characterize negative correlations, the group maps were reconstructed with use of the minimum or mean negative CC values for the

MAX and MEAN approach, respectively.

2.1.4. Visualizing epileptic activity

Patient history

A 20-year-old woman without risk factors for epilepsy suffered from epileptic seizures since age 11. Her seizures began with palpitation feeling and flushing followed by loss of consciousness and distal bilateral hand automatisms. She received all available antiepileptic drugs and numerous drug combinations including phenytoin, carbamazepine, oxcarbamazepine, valproic acid, sulthiam, clobazam, clonazepam, phenobarbital, primidon, vigabatrin, felbamate, ethosuximide, gabapentin, levetiracetam, topiramate, lamotrigine, zonisamide. Due to drug resistance the patient underwent a neurosurgical evaluation in 2001. Neurological examination was normal. The patient's global IQ was 94. High-resolution MRI revealed no structural abnormality. Interictal EEG showed left frontal interictal epileptiform discharges. A left frontal seizure pattern appeared during ictal scalp EEG examination. Ictal SPECT revealed left frontal hyperperfusion in frontomedial and frontobasal regions. Interictal PET examination showed left-sided hypometabolism in the frontopolar, frontobasal, fronto-dorsal, temporopolar areas and in the cingulate gyrus. Electrophysiological examinations using implanted subdural electrode grids suggested a seizure onset in the frontopolar region. On the basis of this examination, she underwent surgical interventions in 2001: the left frontal pole was removed. Because the seizure severity and frequency were not changed postoperatively, a second examination by subdural electrode grids was performed. This suggested a seizure onset posterior to the firs resection. The patient underwent a second operation in 2002: the first and second gyri of her left frontal lobe were removed. She did not become seizure-free, but her seizure semiology completely changed: seizures consisted of right-sided clonus in her mouth

without loss of consciousness. Previous seizure types disappeared. On two occasions they were preceded by strange throat sensation. The postoperatively altered seizure semiology may caused by the ictal spread activating other brain regions than preoperatively. At the time of investigation seizure frequency was 5-30 focal seizures per day (10 in average) lasting for 0.5-2 minutes. She was on carbamazepine and vigabatrin therapy. Similarly to the preoperative ictal recordings, the postoperative ictal scalp EEG showed left fronto-temporal seizure pattern.

Data acquisition

The experiment was conducted with the understanding and the written consent of the patient, and the local ethical committee of University of Pécs approved the experiment. The ictal-fMRI examination was conducted on a clinical scanner operating at 1T (Siemens Magnetom Harmony). A standard Siemens circularly polarized head coil was used for signal excitation and detection. The patient's head was firmly taped to the head coil to prevent involuntary movements. Ictal fMRI study employed a commercial optimized EPI sequence with the following parameters: TR/TE = 2500 ms/80 ms, $\alpha = 90°$, BW 752 Hz, FOV = 210 x 210 mm and matrix 64 x 64 yielding 3.3 x 3.3 mm in-plane resolution, and 12 sections with a thickness of 5 mm and 1 mm gap. With these settings we were able to acquire a good coverage of the whole brain with relatively good temporal resolution of 2.5 seconds. During fMRI the patient was observed by her neurologist. The start and the end of the seizure were detected visually by observing mouth clonus. A set of 250 EPI images, corresponding to an acquisition time of 10m 25s, was acquired including images before, during and after mouth clonus. Some other seizures were also recorded in more sessions, but this was the only session containing relatively stable baseline long enough before and after the seizure. Further, the other fMRI datasets captured during seizure in other sessions

were severely corrupted due to excessive head motion that rendered the data uninterpretable.

Anatomical images were also acquired for identification of brain areas. We applied a 3D FLASH-sequence with the following parameters: TR/TE = 2110 ms/4.38 ms, flip angle 15°, receiver bandwidth 130 Hz, voxel 1.3mm, isotropic.

Data processing

A retrospective motion correction was performed in the k-sapce with an algorithm built in the commercial Siemens BOLD imaging application, and the Realign function of SPM (Friston et al, 1995) was also applied.

First, an internal reference curve was identified by examining the signal alteration of each voxels during the whole acquisition time in the left motor area corresponding to the right mouth clonus. As we were about to use a voxel-by-voxel analysis, a reference signal curve of a particular voxel was selected that showed relatively flat baseline, a symmetric signal peak and an intensity alteration of 9%.

The cross-correlation function using the internal reference curve was applied to assign a correlation coefficient value to each pixel. Cross-correlation function examines the similarity between the signal alteration in a given voxel and a reference curve. The reference curve was also shifted scan by scan to examine the correlation at each time point, thus all signal curve showing activation could be determined regardless of the time of activation. The histograms of the correlation coefficients showed a distribution different from Gaussian indicating that activation occurred (Kleinschmitd et al, 1995; Baudewig et al, 2003). Active pixels were pointed out if their correlation coefficients exceeded the 99.85% (equal to p value of 0.0015) percentile rank of the fitted Gaussian function, thus showing the local maxima of the corresponding activation clusters. In a second step,

neighboring pixels were iteratively added to the corresponding activation clusters as long as their correlation coefficient exceeded the 95% percentile rank (equal to p value of 0.05). The correlation coefficients corresponding to p value of 0.0015 and 0.05 were 0.778 and 0.445, respectively. A detailed description of the analysis using the noise distribution of the correlation coefficients can be found above.

As we had to define the first rising point of the BOLD signal peak in the identified activation clusters, we used the widely accepted upper three-sigma rule (i.e. three times standard deviation) to determine a threshold from the value of the baseline (i.e. first 20 scans). According to our definition this point can show the beginning of the hemodynamic alteration, thus the start of a putative epileptic activity in the respective brain area. The exact locations of the activated clusters were identified by an overlay of anatomical areas using IBASPM (Fischl et al, 2004).

A color-coded lag-time map was produced to demonstrate the spread (i.e. the order of activation) of the epileptic activity. It shows the rising points of BOLD signal peaks in each activation cluster during examination.

2.1.5. Combining with DTI-FT

Case history

A middle-aged female patient had suffered a traffic accident. She had fallen out of a vehicle at high speed, hitting her head twice, injured with combined acceleration-deceleration mechanism. She had lost her conscious at once, after resuscitation she had been transported to the hospital in state of Glasgow Coma Scale 4 with stable cardiovascular system.

CT-examination had resulted in opened impression fracture on the left frontoparietal region, bilateral contusion on the frontobasal region and on the left convexity.

In the first step, extensive decompression craniectomy had been carried out on the left due to the increase in intracranial pressure. After four weeks of intensive therapy providing satisfactory cerebral blood flow, the patient had not regained her conscious; spontaneous movements in her extremities had not been observed, either.

Two months after her admission, she was transported to the regional rehabilitation center for further treatment. At that time, her cycle of sleeping and awakening came back. She reacted to pain- and auditory stimuli with bilateral eye-opening and mass-flexion on upper and lower extremities. Mastication and palmomental sign were observed representing degradation; in addition pyramidal signs and mild increase in muscle tone was present.

EEG-examination, conduced on the same day as fMRI and DTI, showed diffuse cortical deceleration and decreased background activity on the left. Somatosensory Evoked Potentials referred to sever brain stem damage; Motor Evoked Potentials resulted no response on periphery with stimulating the motor cortex on any side.

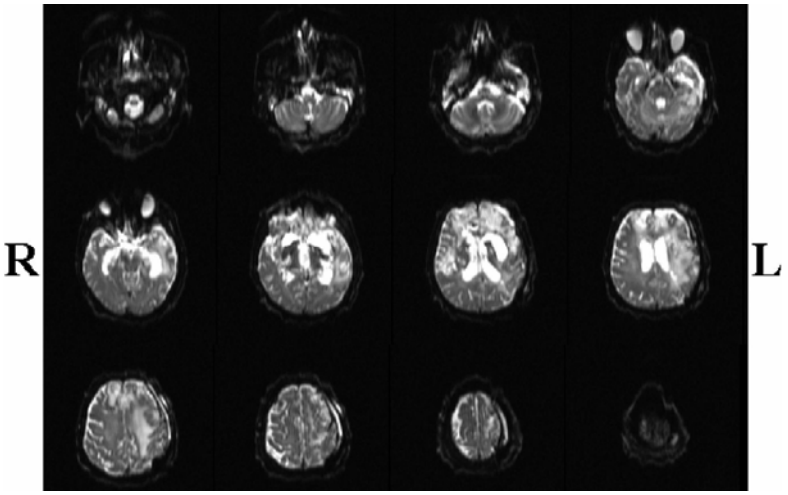

Figure 7. *T_2-weighted images.* Bilateral post contusion damages can be observed especially in the frontal and parietal lobes. Damages on the left are more severe: cyst communicating with the lateral ventricle, increased signal intensity in the temporal and parietal lobes.

T_2-weighted MR images demonstrated severe structural damage in the subcortical region and in brain stem (Figure 7).

FMRI

In our clinic, fMRI has been routinely used since 2005 October. Due to the unconsciousness of the patient, fMRI of passive finger movement (PFM) (Holloway et al,

2000) was applied on both sides to visualize activity in the senso-motor cortex bilaterally. Examination was conducted on a clinical system operating at 1T (Siemens Magnetom Harmony, Erlangen, Germany). A standard Siemens circularly polarized head coil was used for signal excitation and detection. Functional studies employed an EPI sequence as supplied by the manufacturer with the following parameters: TR/TE = 2500 ms/80 ms, α = 90°, BW = 752 Hz, FOV = 192 × 192 mm and matrix 64 × 64 yielding 3 × 3 mm in-plane resolution, and 16 sections with a thickness of 3 mm and 1 mm gap. Although, condition of the patient was stable, during examination, her cardiac function, breathing and blood oxygen saturation were also monitored.

Analysis was carried on under MatLab 6.5 with the software using TTC proved to be optimal for datasets acquired al 1T. As upper and lower thresholds, p = 0.001 and p = 0.05 were used.

DTI-FT

DTI was accomplished on the same scanner operating at 1T with the same head coil, as mentioned above. A sequence supplied by Siemens in the framework of IDEA (Schepers, Schnell and Vroom, 1999) was applied with the following parameters: TR/TE = 7300 ms/112 ms, FOV = 256 × 256 mm and matrix 128 × 128 yielding 2 × 2 mm in-plane resolution with a thickness of 4 mm, b = 600 $mm^{-2}s$, number of diffusion directions: 16. Additional scans were also acquired with the same parameter but b = 0 $mm^{-2}s$ resulting standard T_2-weighted images necessary to DT-evaluation. 34 axial slices were obtained; and to increase SNR, 12 repetitions were also applied.

DTIStudio 2.4 (Mori S, Hangyi J and Kegang H. http://lbam.med.jhmi.edu/DTIuser/DTIuser.asp) was used for evaluation, which can combine the repetitions to increase quality of the results. T_2-weighted images of the

repetitions (see above) were combined separately too, and every third slice was presented to show pathology (Figure 7). For the first step of the evaluation, DT-values were calculated voxel wise, and voxels were marked with different colors according to the directionality of their anisotropy (cranio-caudal – blue, sagittal – green, medio-lateral – red). In the next step, neural fibers were tracked along DTs. Here thresholds had to be determined to tell the program which voxels belong to each fiber: FT began at FA of 0.15 in a ROI defined and stopped when there were no voxel with a minimum FA of 0.15 and a maximum declination of 0-70º. As we were interested especially in the long tracts, ROIs were selected in more areas marked with blue (cranio-caudal directionality). Each fibers passing through the given ROI were marked with different colors. Statistical analyses about number and length of fibers were also conducted.

DTI-examination and evaluation were also accomplished on a healthy volunteer for the sake of comparison.

2.2. Recording neural activities by means of SPECT using modified SISCOM-analysis

The patient

The 22-year-old female university student was born with a right-sided spastic hemiparesis due to a perinatal injury. Although the strength of the right limbs normalized, the abnormal posture of the right upper limb was noticed at the age of 2 months, developing to a drug-refractory and painful secondary hemidystonia. The locomotive and intellectual development was otherwise normal.

Brain MRI revealed a 4x15x18mm lesion in the left globus pallidum (GP). At age 22, she underwent a microelectrode-guided Medtronic quadripolar 3389 Deep Brain Stimulation (DBS) electrode implantation into the left posteroventral GP interna (GPi) without perioperative complications. As a part of routine neurosurgical evaluation, fMRI was

applied to visualize her speech centers (Woermann et al, 2003). The patient has given written informed consent to the whole surgical procedure, pre- and postsurgical examinations and publication of the present case report, whereas the study was also approved by the Local Ethical Committee.

Stimulation settings

On the first postoperative day, contact 1 was activated in a monopolar mode (C+1-, 120μs, 130Hz, 3.2V) without any adverse reactions. The patient was admitted to the Neurological ward on the 3rd postoperative week to learn the use of patient controller. During the testing of electrodes, we noticed that the monopolar stimulation of contact 0 with the amplitude exceeding 2.7V could elicit several Déjà Vu (DV) episodes. As the turning on or off the stimulation had an immediate effect on this experience, we assumed it to be a stimulation-related adverse reaction. The impedance of contact 0 (C+0-, 3.2V, 120μs, 130Hz) was 562 Ohms.

SPECT

The current safety regulations do not permit using fMRI during DBS (Kovacs et al, 2006). Morever, fMRI is not well suited for detecting rare, longer events (see 1.4). Therefore, we performed 99mTc HMPAO-SPECT to study the pathophysiology of DV because 99mTc-hexamethylpropyleneamineoxime has a binding of 2-10 minutes (Andersen, 1989).

The SPECT acquisition was performed 1 month postoperatively. To exclude the long-term duration effect of DBS, the *'baseline' SPECT* was obtained during the *normal stimulation* of contact 1 (C+1-, 3.2V, 120μs, 130Hz). For studying the pathophysiology behind DV, three days later we stimulated simultaneously both contact 0 and 1 (C+0-1-, 120μs, 130Hz, 3.2V referred to as *DV-inducing stimulation*). Analogously to epilepsy studies we defined

this setting as *'ictal' SPECT*.

As the 99m-TcHMPAO tracer (750MBq) was administered immediately after starting the DV-inducing stimulation and the patient experienced four DV experiences during the first 5 minutes of stimulation, we assumed that the tracer binding in the 'ictal' SPECT represented the combination of acute DV induction and normal pallidal stimulation. Therefore, the subtraction of 'baseline' from the 'ictal' SPECT images theoretically corresponded only to the areas activated during DV experience.

SISCOM

The comparison of 'baseline' and 'ictal' SPECT was performed with analysis based on SISCOM method used in presurgical evaluation of epilepsy (O'Brien et al, 1998) with the following steps: (1) spatially normalizing the ictal and interictal (baseline) SPECT scans to the MNI-space (Colins; 1994); (2) for each study, normalizing the mean cerebral pixel intensities to a mean cerebral intensity of 100 of each study; (3) subtracting the normalized modified 'baseline' SPECT-image from the normalized modified 'ictal' SPECT-image to derive the difference; (4) thresholding the subtraction image using similar technique to that in TTC to display pixels with significant difference and (5) overlaying the image showing only significant differences onto the anatomical MR image spatially normalized to the MNI-space.

3. Recording neural activities by means of MRI at low magnetic field

3.1. Optimizing parameters at low magnetic field

3.1.1. Results

3.1.1.1. Basic paradigms and clinical application

FMRI of healthy volunteers

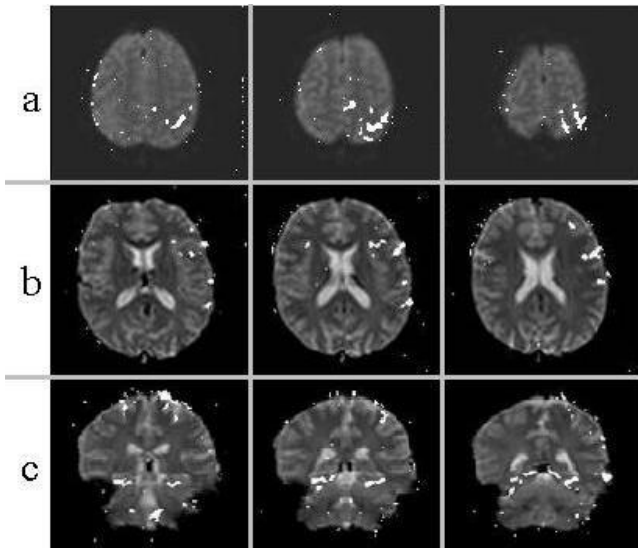

Figure 8. Activation maps resulted from different paradigms overlaid onto EPI images. (a) SFO, (b) IWG, (c) mental navigation

Figure 8 shows the results of the evaluation of the FMRI datasets overlaid onto EPI-slices showing the areas relevant for the paradigm. Voxels showing significant ($z > 3.5$) signal elevations during the active phase are represented with white pixels. Concurrent activation of a cluster of at least 4 neighboring voxels can be assumed to represent a true spot of activation. Other clusters containing less and situated scattered are artefacts most likely.

Picture 8.a visualizes prae- and postcentral gyri on the left hemisphere referring to the activity during right-sided SFO. Picture 8.b demonstrates the activation Broca's and Wernicke's areas resulted from IWG. On Picture 8.c, we can observe activities bilaterally in the hippocampus, the fornix and the parietal cortex resulted from mental navigation task.

3.1.1.2. Comparative study at 1T and 3T

Despite considerable intra- and intersubject variability in the activation maps regardless of field strength and paradigm, our results yielded consistent findings with respect to field strength and post-processing strategy. The upper parts of Picture 9.a show the activation

maps of a single subject obtained for the IWG paradigm. While at 1 T the single-subject TTC analysis (Picture 9.a, top rows) yielded more activated pixels in the Broca's area than SPM (Picture 9.a, middle rows), this example revealed approximately the same amount of activation at 3 T for both methods. This latter observation also holds true for a SPM group analysis averaging all word generation data sets across subjects (Picture 9.a, bottom rows). Picture 9.b displays activation maps for executing the SFO task. Again, at 1 T the single-subject TTC analysis resulted in much more extended activations in the primary sensorimotor cortex and supplementary motor cortex than the single-subject SPM approach. At 3 T the activation maps for both methods were equivalent as were the SPM group analyses at both field strengths. Representative results for the passive finger movement paradigm in another subject are demonstrated in Picture 9.c. In this case the single-subject TTC analysis yielded even more activated voxels at 1 T than at 3 T (similar to Picture 9.b), whereas the single-subject SPM approach again showed much less activation at the lower field strength. In agreement with the other paradigms, the SPM

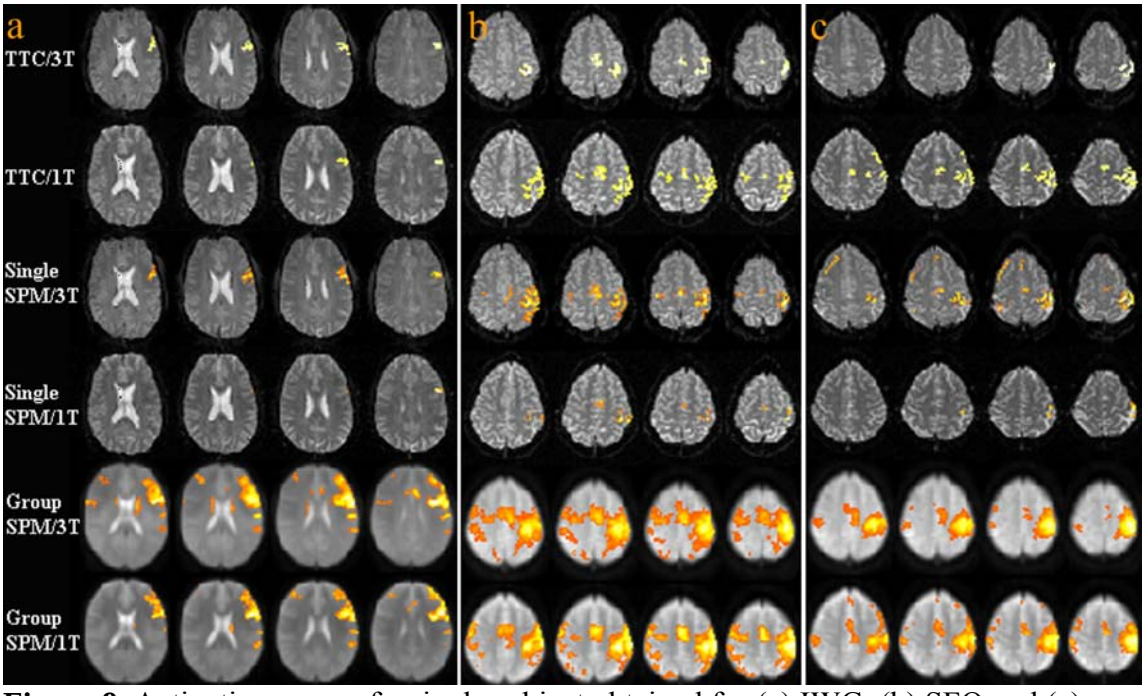

Figure 9. Activation maps of a single subject obtained for (a) IWG, (b) SFO and (c) PFM at 1 T and 3 T and for different analysis methods. (Top rows) Single-subject TTC analysis, (middle rows) single-subject SPM analysis, and (bottom rows) SPM group analysis (8 subjects).

group analyses were almost undistinguishable at both field strengths.

Table 2. Numbers of activated voxels			
	3T	**1T**	**3T/1T**
IWG			
SS[1] TTC	40 ± 43	38 ± 24*	1.05
SS SPM	39 ± 38	11 ± 8	3.55
Group SPM	567	421	1.35
SFO			
SS TTC	176 ± 117	157 ± 42**	1.12
SS SPM	150 ± 67	52 ± 25	2.88
Group SPM	781	764	1.02
PFM			
SS TTC	131 ± 58	135 ± 51**	
SS SPM	133 ± 38	41 ± 24	3.24
Group SPM	598	580	1.03
[1]SS = single-subject analysis, * $p < 0.005$ and ** $p < 0.0005$ in comparison with SS SPM			

Table 2 summarizes the mean number of activated voxels in the Broca's and sensorimotor regions. For all paradigms, the TTC and SPM single-subject analyses at 3 T gave similar results, whereas the SPM approach failed to reveal similar activations at 1 T but resulted in about 3-fold lower numbers of activated voxels. The single-subject TTC approach, however, identified a similar number of activated voxels for all paradigms at both field strengths. Similar results for the SPM approach could only be obtained when applying it to a group analysis.

The mean SNR of all images at 3 T (265±46) was 4.5 times larger than at 1 T (59±7) because of both the larger spin polarization and an improved radiofrequency coil design. The corresponding MRI signal intensities of all activated pixels in the Broca's area and sensorimotor cortex are shown in Figure 10 as mean curves averaged across subjects. The

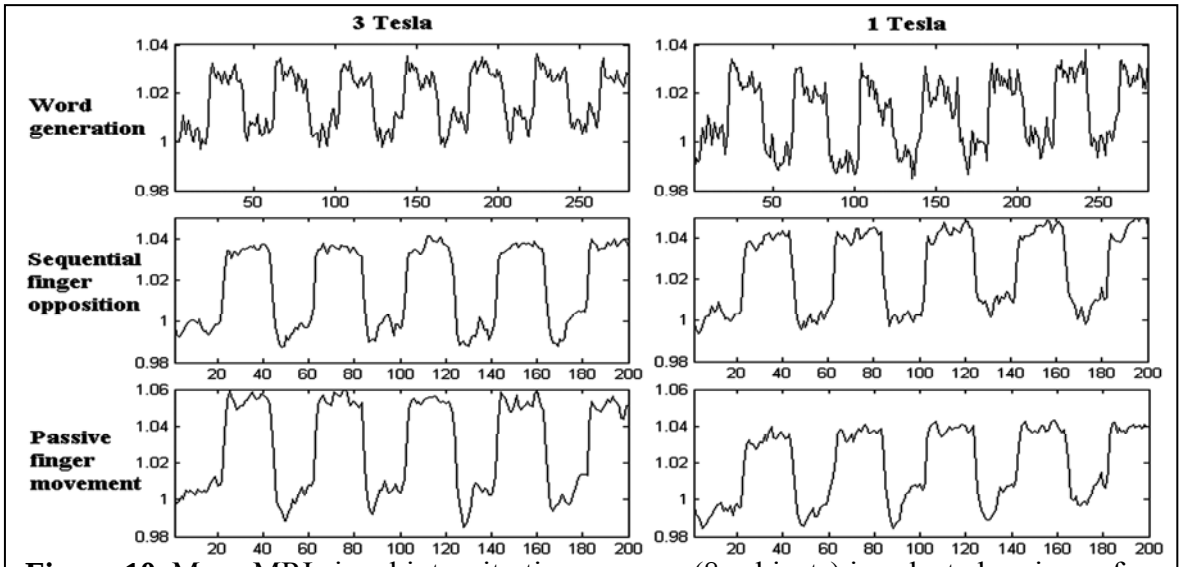

Figure 10. Mean MRI signal intensity time courses (8 subjects) in selected regions of interest for IWG, SFO, and PFM at 3 T and 1 T.

magnitudes of the signal changes for word generation (3%) and SFO (3.5%) were found to be identical at both field strengths. For passive finger movement the mean signal change in the sensorimotor region was 4.5% at 1 T and 6% at 3 T.

3.1.2. Discussion

Low field MRI systems tend to spread mostly in neurosurgery and render possible fMRI or DTI in the operating room. Despite some successful demonstrations of feasibility of intraoperative fMRI (Azmi et al, 2007; Schulder, Azmi and Biswal, 2003; Gering and Weber, 1998), appropriate fMRI sequences (fluid attenuated inversion recovery (Hajnal et al, 1993) or gradient echo) and mostly post-processing strategies at low magnetic field require more investigation to cope with inherently low signal to noise ratio.

So far, published reports on a comparison of functional MRI of human brain activation at different field strengths (Gati et al, 1997; Turner et al, 1993; Krasnow et al, 2003; Fera et al, 2004; Krüger, Kastrup and Glover, 2001) unanimously conclude that a higher field is preferable. Unfortunately, however, at least part of these studies was compromised by the use of special radiofrequency coils (Turner et al, 1993); or special MRI sequences, not generally available for routine clinical work, were applied (Krasnow et al, 2003; Krüger, Kastrup and Glover, 2001). The purpose of our study was to make a fair comparison by completely relying on commercial coils and standard EPI sequences. Moreover, experiments were performed at a typical spatial resolution and for clinically relevant paradigms that map eloquent brain areas.

Not surprisingly, the data resulted in similar percent MRI signal changes in response to word generation and sequential finger opposition at 1 T and 3 T. Only a moderate increase was observed for passive finger movements at 3 T. It is well known that – for a given voxel size – the sensitivity to (microscopic) susceptibility differences primarily depends on

the gradient echo time. Thus, the increase in sensitivity to susceptibility differences at a higher magnetic field strength – for a given echo time – may well be compensated for by increasing the echo time at a lower field. This effect has also previously been reported by comparing functional MRI studies at 1.5 T and 3 T (Fera et al, 2004; Krüger, Kastrup and Glover, 2001). For instance, Krüger and coworkers measured similar BOLD signal changes for a visual and motor task at 1.5 T and 3 T. The large intrasubject variability of fMRI data (Havel et al, 2006) is another well-known feature and obvious on Figure 9. Despite extreme examples such as a subject who produced more activation at 1 T than at 3 T (Pictures 9.b and c, TTC), our results yielded consistent findings with respect to the post-processing strategies.

As a novel finding, the present results clearly indicate the influence of the method chosen for post-processing and in particular for the statistical evaluation of significant activations. While both the single-subject TTC and SPM analyses yielded similar numbers of activated voxels at 3 T, the SPM approach failed in detecting such activations at 1 T. In fact, the number of activated voxels was reduced by about a factor of 3. On the contrary, the TTC approach readily identified similar activations at both field strengths. This discrepancy may be best explained by the use of two physiologically justified thresholds that reflect the individual noise in the distribution of correlation coefficients for each trial and subject. In other words, TTC activation maps take into account the intrasubject variability not identified by SPM (compare Picture 9.b, first four rows). The concept of two thresholds accounts for the fact that highly significant activation centers or nuclei (pixels identified by a high threshold) are usually surrounded by directly neighboring pixels that are also activated but at a somewhat lower statistical significance (area delineation above a lower threshold). This combined strategy appears to be much more robust than the single threshold employed by SPM in situations of limited SNR. Together with suitably adjusted

echo times, it obviously compensates to a large degree for a lower functional contrast-to-noise than principally available at higher fields. The lack of similar observations in previously published reports may possibly be explained by the fact that – to the best of our knowledge – all such studies were analyzed with SPM or other methods using only a single threshold. It should be emphasized that the gain in the number of activated pixels for TTC as compared to SPM is not the result of the putative generation of more false positive activations. Instead, the opposite is true, as TTC uses a low statistical threshold of $p = 0.05$ exclusively for limiting the extent of activations that are originally identified with a threshold of $p = 0.0001$, whereas SPM relies on $p = 0.05$ throughout. It should be also noted that statistical threshold of $p = 0.05$ is differently defined in SPM and TTC. Otherwise more similar number of activated pixels would occur in both post-processing strategies.

The present findings offer two more consequences. Firstly, they again demonstrate the particular strength of the SPM approach for group analyses, and secondly, they lead to the recommendation that the good SNR at higher fields is best exploited by improving the spatial resolution. Or conversely, limitations of functional MRI studies at a low magnetic field strength are to be expected in those cases that require higher spatial resolution and/or better sensitivity for the detection of subtle MRI responses to more sophisticated cognitive paradigms. In other words, scanners in our country operating at low field are capable to visualize brain activation during most of the clinically relevant paradigms.

3.2. Diagnostic studies (neurosurgical planning and functional neuronavigation)

3.2.1. Results

Preoperative fMRI examination

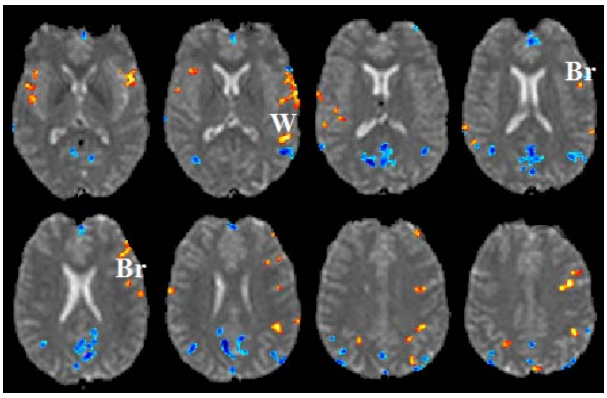

Figure 11. *Preoperative fMRI (IWG).*
Br: Broca's area; W: Wernicke's area.

Figure 11 shows an example of activation maps resulted from the paradigm of IWG as a part of a neurosurgical evaluation. The 29-year-old female patient suffered from severe headache attacks. Neurological examinations revealed TLE, and then neuroradiological examinations found low-grade glioma as the epileptogene lesion. The patient was admitted for evaluation for epilepsy surgery to remove the tumor as well as the anterior part of her left temporal lobe.

Functional dataset was analyzed with TTC approach (see above). Activations are represented with colors from red to yellow corresponding to the strength of the activation, while deactivations are represented similarly with colors from light to dark blue. Results revealed the left hemisphere as dominant because of the location of activations in the level of Broca's area. The Broca's area was found in the triangular and opercular part of the inferior frontal gyrus on the left, while the Wernicke's area was visualized in the angular gyrus on the left.

Operation with the help of functional neuronavigation

Figure 12 demonstrates functional surgical guidance provided for the operation of the female patient mentioned above. Slices are represented not in the standard (sagittal, axial and coronal) view, but according to the location of the pointer (blue) oblique to the

standard axes. Therefore slices in the pictures are distorted a bit. Activation map of IWG overlaid onto the anatomical images was used. Exploration (yellow lines) was planned preoperatively taking account of the localization of the eloquent areas. With the help of functional neuronavigation neurosurgeon could monitor the location of eloquent areas in every step and extend radicality to the required extent. Operation was accompanied with no morbidity. Pathology on the sample taken during the operation resulted astrocytoma WHO grade II.

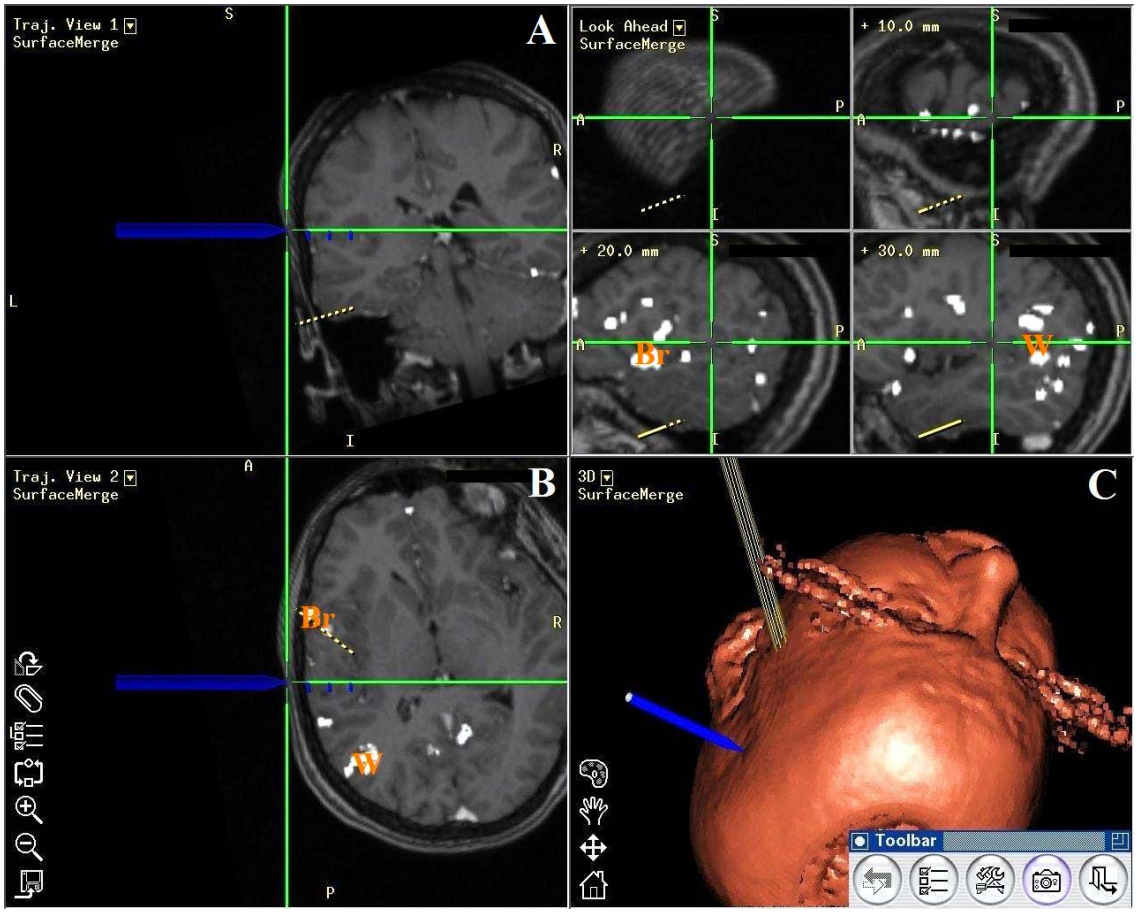

Figure 12. *Functional neuronavigation.* Br: Broca's area; W: Wernicke's area. Yellow lines represent the planned way of exploration, while the blue pointers show the current place of the pointer in the surgeon's hand.
Picture A and B show the volume in coronal and axial views, while picture C shows it in 3D space. The four smaller pictures (upper right corner) show sagittal slices 0, 10, 20 and 30 mm deep from the pointer.

Control examinations

Three weeks after the surgery patient was in a good general condition: she reported no

headache attacks, became seizure-free and could return to her normal daily routines.

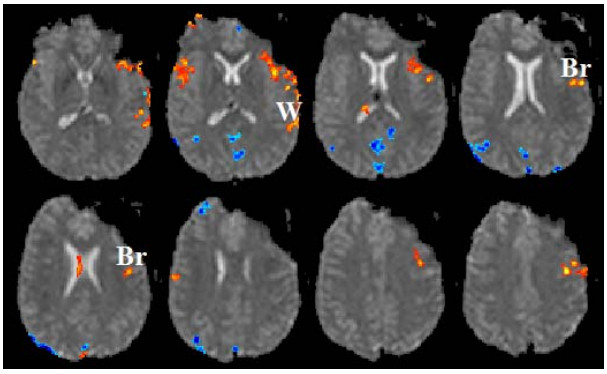

Figure 13. *Postoperative fMRI (IWG).*
Br: Broca's area; W: Wernicke's area.

Figure 13 shows the result of the postoperative fMRI with IWG overlaid onto the EPI images. The signal void, due to increased susceptibility, is apparent at the site of the brain parenchyma resection disturbing slightly the identification of activations. Despite of it and the positioning of the slices not totally identical to that of the preoperative fMRI, slices and activations on Figure 11 and 13 can be easily matched. As a result of comparison (a) activations were visualized on the same spot pre- and postoperatively; (b) functional intensity in areas close to the intervention has increased; (c) functional intensity of the eloquent areas has not decreased.

Neuropsychological examination

Preoperative tests demonstrated no deficit in mental performance (ACE = 96/100).

Tests acquired three weeks postoperatively revealed minimum decrease in mental performance relative to that of preoperatively giving results (ACE = 90/100) still over threshold to normal (80/100). Token-test accomplished to examine speech recognition specifically resulted in latent decrease (59/62).

3.2.2. Discussion

FMRI as a part of routine neurosurgical evaluation has been set up for a long time in abroad. In Hungary, we was the first who uses it in a clinical routine; and 114 sessions with 48 patients examined and operated based on the results surely prove, that (a) fMRI of clinically relevant paradigms can be acquired and analyzed with good quality even at 1T

(b) visualizing the eloquent areas with good accuracy, and (c) can be applied for neurosurgical planning and functional neuronavigation. (d) Finally, as we accomplished the examinations on a clinical scanner – operating at 1T – available in all Hungary; this presented method can be widely applied.

Evaluation

Despite of the good availability of some software-packages for fMRI analysis, most of them are not simple, fast and flexible enough to become the best candidate for neurosurgical evaluation. TTC, however, was proved to be fast and accurate enough in comparison with other software packages; and – more importantly – demonstrated to be beneficial especially at low field (see 3.1.1.2). In addition its thresholding approach is transparent and flexible enough to meet the requirements. It is easy to automate and provides a handy tool for neuroradiologists in routine examinations. Moreover, results superimposed on the anatomical images can be exported into DICOM format able to be uploaded onto the neuronavigation system to provide more accurate and flexible real-time functional guidance for the neurosurgeon.

Functional neuronavigation

In neurosurgical evaluation, fMRI offers a valuable help. As activation map(s) can be overlaid onto the anatomical images, exploration can be planned with great accuracy and safety to avoid any damage on eloquent areas. With its help, invasive preoperative examinations such as Wada-tests can be substituted; and most of the cases operation on wakeful patient may become unnecessary, avoiding a heavy load on both patient and doctors, as well as ensuring the application of precise microsurgery.

Tumors like astrocytoma in WHO grade II tends to oncological progression (Molnár,

2004), so it is important to achieve the greatest possible radicality provided by real-time functional guidance.

3.3. A novel group analysis

3.3.1. Results

Figure 14 shows the group distributions of CC values from all subjects and sections for the two tasks studied. When comparing the actual distribution (dotted lines) and the estimated noise distribution (solid lines), active finger movements were mainly characterized by deviations in the positive CC range indicating activations. The word generation paradigm revealed deviations for both highly positive and negative CC values that correspond to activated and deactivated voxels, respectively.

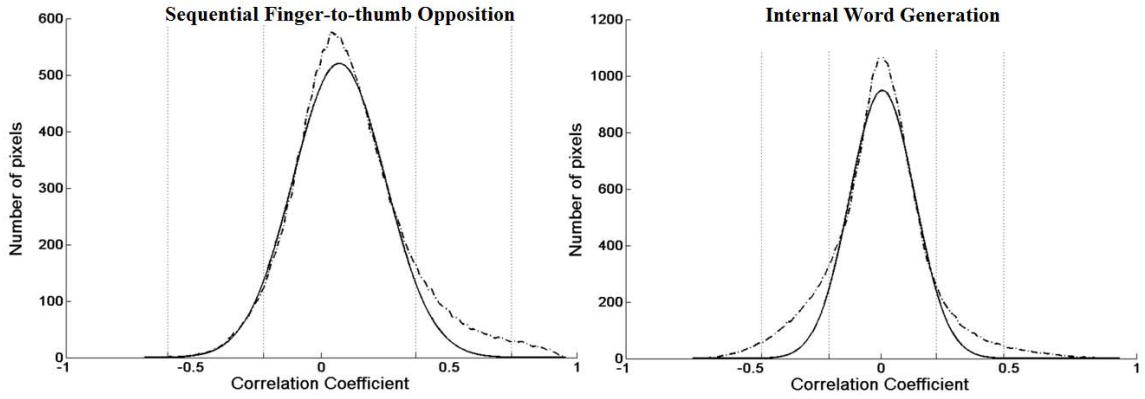

Figure 14. *Group distributions of CC values*
from all subjects and sections (dotted line) for SFO and IWG.
solid lines: fit of a Gaussian function to the central portion of the CC distributions
vertical lines: 99.99 and 95 percentile ranks of the Gaussian distribution

Figure 15 summarizes group activation maps obtained by SPM and TTC for IWG and SFO (4 sections each), respectively. In either case, the first row shows SPM group maps, while the bottom two rows refer to the group maps obtained with TTC MAX and TTC MEAN, respectively. All post-processing methods identified the sensorimotor and supplementary motor areas for the motor task as wells as the Broca's region for the word generation paradigm. The locations and the extent of activations/deactivations were similar for the maps analyzed with SPM and TTC MAX, whereas activations/deactivations appeared

much more restricted when using the TTC MEAN approach. Even TTC MAX demonstrates activation in a somewhat "clearer" way eliminating one of the biggest drawbacks of SPM: SPM visualizes a lot of scattered "activation" along the brain even using the highly conservative threshold of p = 0.05 FWE corrected. Most of these scattered pixels cannot be seen on TTC MAX. Some of the "activation" clusters assumed to be false positive (white arrowhead) were examined looking the signal alterations in all of the subjects, which proved our assumption.

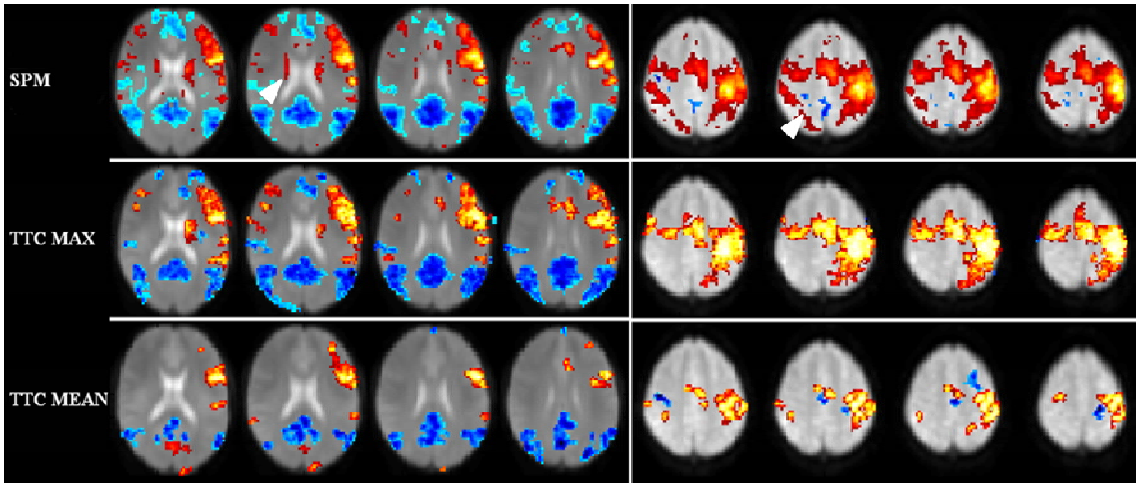

Figure 15. *Group activation maps* obtained for IWG (left column) and SFO of the right hand (right column). Group maps are calculated with SPM, TCC MAX and TTC MEAN approaches. Activations and deactivations are indicated by red and blue colors, respectively.
white arrowhead: false positive activation not showed by TTC.

A brief quantitative comparison of activated voxels obtained for silent word generation with use of SPM, TTC MAX, and TTC MEAN is given in Table 3 and supports the qualitative findings from the images.

Table 3. Total activations and deactivations obtained for IWG with SPM, TTC MAX, and TTC MEAN

	SPM	**TTC MAX**	**TTC MEAN**
# Activated voxels	4326	5292	2449
# Deactivated voxels	7268	6439	2814

3.3.2. Discussion

Despite a widespread acceptance and availability of SPM, the analysis of fMRI data sets remains a field open for improvements. The idea of this work is not to design a new

mathematical framework, but to describe a simple and transparent technique.

While most of the proposed analysis strategies rely on a single statistical threshold (sometimes supplemented by a cluster threshold), the key of the TTC method is a combination of two thresholds in a physiologically meaningful manner. In more detail, the resulting advantageous features may be explained as follows. First of all, in the absence of a functional challenge, correlation analyses have been demonstrated to result in a symmetric distribution of CC values (centered around zero), which may be characterized by a Gaussian function (Kleinschmidt et al., 1995). This noise distribution reflects physiologic fluctuations and/or 'resting state' brain activity of the subject and as such may vary in broadness from experiment to experiment. It is therefore mandatory to estimate the noise distribution for the actual fMRI acquisition to be analyzed. This is accomplished by restricting the fit to the central portion of the actual CC distribution which contains only low CC values of voxels not engaged in task performance. This procedure ensures substantial robustness of the TTC analysis and certainly facilitates intertrial comparisons by removing systemic alterations not related to the interrogated functional state.

Secondly, the actual CC distribution is rescaled in percentile ranks of the noise distribution. This step is followed by an automatic definition of two statistical thresholds which are tightly linked by neighborhood principles when used for calculation of an activation map. While the upper threshold focuses on the identification of highly significant activations, the lower threshold is only used to better delineate their spatial extent rather than to incorporate new activations of low significance. This strategy may be characterized as defining the mountain around its peak. It yields robust statistical parametric maps of activated voxels with both high specificity and sensitivity under the assumption that voxels within a truly activated area bear a tight topographic relationship to a smaller number of voxels which exceed a threshold related to a very low type-one error

probability (false positives). The method should not be mistaken for a `cluster analysis' that relies on assumptions about the cluster size in relation to the image resolution. Specifically, the spatial response delineation used here does not exclude small – even single voxel – activations which are necessarily omitted in a conventional cluster analysis.

Two different group CC maps have been tested (bottom rows of Figure 15). A maximum sensitivity is obtained for the TTC MAX approach which is based on group CC maps that incorporate the maximum (or minimum) CC values observed in the entire group of subjects. The general appearance of these maps is similar to what may be obtained with a standard SPM analysis (top row of Figure 15), but demonstrating activations in a somewhat "clearer" way eliminating a lot of scattered "activation". Conversely, when using the mean value rather than the extreme CC values, the TTC MEAN results appear more conservative and demonstrate activated (or deactivated) clusters in a very restrictive manner. Taken together, the TTC MAX approach may include voxels that are active in only few of the subjects (or even a single subject with a single but very high CC value), whereas the TTC MEAN approach relies on activations more common to the group (or in most of the subjects yielding a high mean CC value). In this sense the TTC MAX but TTC MEAN even more successfully eliminates false positive activations.

3.3.3. Example – Taste fMRI at 1T

Figure 16 demonstrates a possible application of TTC group analysis (TTC G).

Six healthy student (age around 20) have taken part in this pilot experiment. Via small tubes distillated (tasteless) water and distillated water containing sucrose and chinin for sweet and bitter taste (tasteful) were injected into their mouth. During fMRI with the usual parameters at 1T (see 2.1.2), 5-5 ml of tasteless and tasteful fluid were administered in control and active phases, respectively; and subjects had to savor both. Swallowing was

allowed just in the end of the phases.

After standard pre-processing steps (motion correction with Realign, normalization into MNI space, smoothing with Gauss-filter with FWHM of 5 mm) with SPM5, datasets were analyzed with TTC G MAX for the sake of increased sensitivity. Activation maps were superimposed on an anatomical image normalized into MNI space.

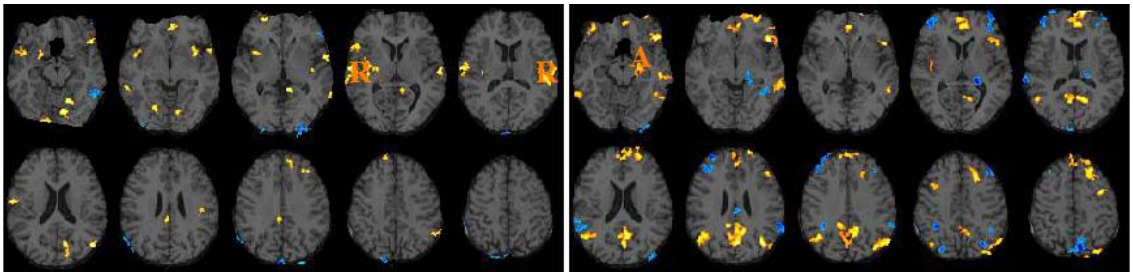

Figure 16. *Taste fMRI at 1T.* Group activation maps obtained for sweet (left column) and bitter (right column) tastes. Group maps are calculated with TCC MAX approach. Activations and deactivations are indicated by red and blue colors, respectively.
R: Rolandic operculum; A: Amygdala

As it can be observed on Figure 16; insula, anterior and posterior cingulated cortex and other part of the limbic system and sensory areas for tasting were activated in both paradigms. In case of sweet taste, however, pronounced bilateral activation of Rolandic operculum responsible for pleasantness (Haase et al, 2007) can be noticed on the left picture of Figure 16. On the right, the activation of the amygdala is demonstrated referring to unpleasantness of bitter taste (Zald, Hagen and Pardo, 2002).

3.4. Visualizing epileptic activity

3.4.1. Results

Mouth cloni were observed during the examination from scan 87 (3m 37,5s) to scan 185 (7m 42,5s). Realign function of the SPM provided maximum values of 0.2mm and 0.4° for residual translational and rotational movements, respectively. Seizure involved only mouth clonus, hence we observed no rough movement via cine loop.

It is obvious that surgical interventions had considerable effect on images (Figures 17, 18). The signal void due to increased susceptibility is apparent at the place of brain parenchyma

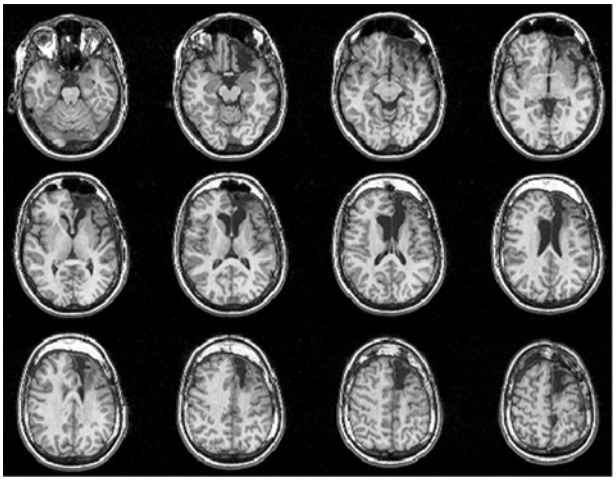

Figure 17. *High resolution anatomical images coregistered to fMRI.* Signs of previous operations are visible in the left frontal lobe.

resection and also close to burr holes used for craniotomies. The rising points of BOLD signals corresponding to the activated areas are color coded according to time and displayed in Figure 18.

Nine activated regions were selected and presented in Figure 19 to

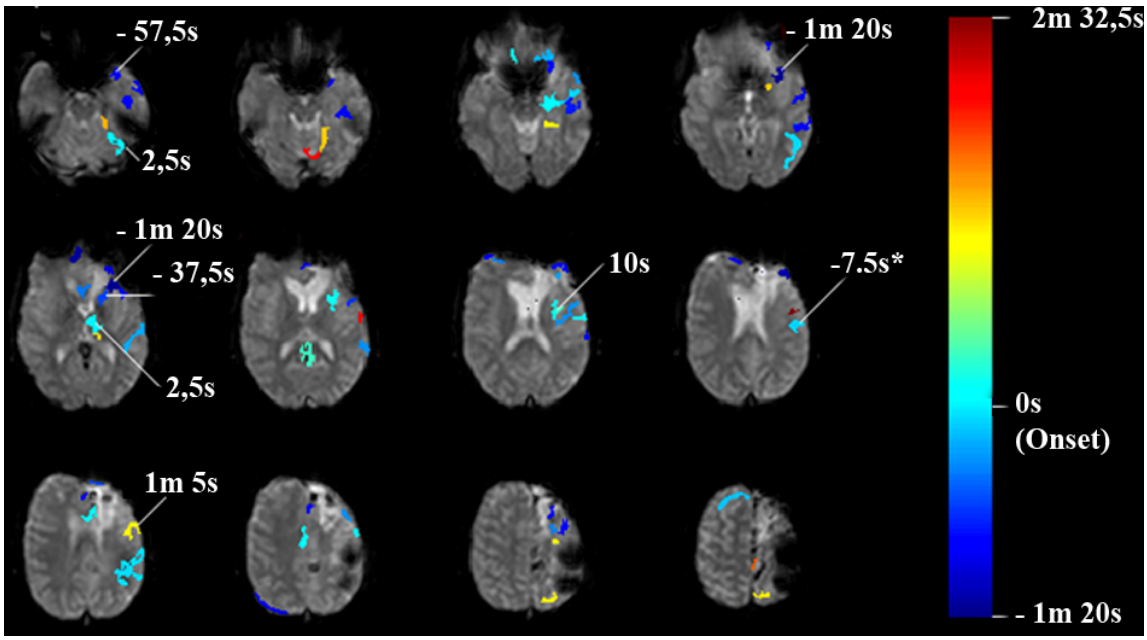

Figure 18. *Lag-time map shows the sequence of activation during the examined seizure.* Colors indicate the activation time relative to seizure onset. Nine regions are labeled with accurate activation time relative to seizure onset. Their BOLD signal changes are demonstrated in Figure 19.
*: motor area of the face.

demonstrate hemodynamic changes. The regions can be identified on Figure 18 by the same activation time appearing on color-coded lag-time maps. The rising point of the BOLD signal is indicated with vertical line while the box above the horizontal axis shows the time of the clinical seizure. The relative signal alteration was about 9% in the active brain regions. The hemodynamic change generally lasted for three minutes from the rising

point to reach the maximum and a bit shorter to fall back to the baseline. It can be clearly seen that the lower part of the insular cortex was activated first and its signal alteration preceded the clinical beginning of the seizure (i.e. mouth clonus) by more than one minute (Figures 18, 19). Most of the activations started before clinical seizure onset. The activation corresponding to the motor area of the right face showed only a 7.5s long pre-ictal phase. However, for instance, the upper part of the insular cortex activated 90 s later than the lower part and showed post-ictal activation (Figure 19). BOLD signal alteration was also observed in the left caudate nucleus, left thalamus, along with various areas of the left cerebral and cerebellar hemisphere (Figure 18). MRI signals form contralateral, non-activated regions showed a relatively flat baseline during the whole investigation (Figure 19).

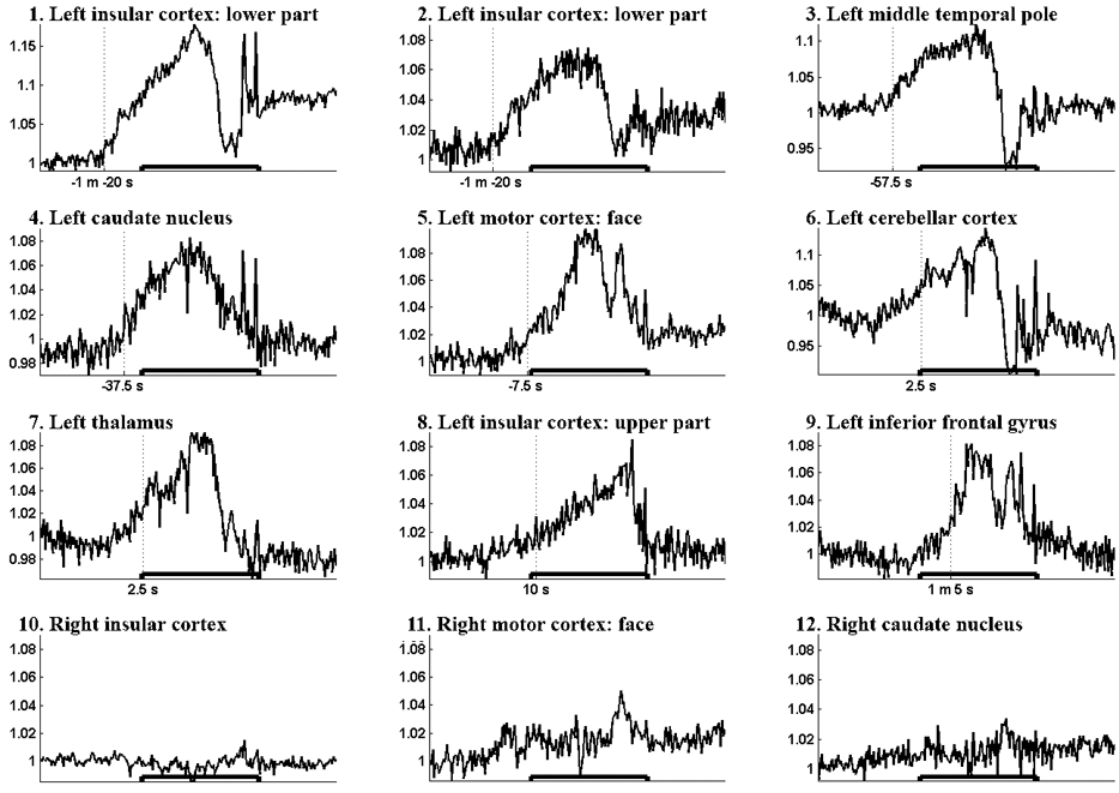

Figure 19. *The BOLD signal alterations of nine activation clusters labeled on Fig 19.* The box above the horizontal axis indicates the length of the seizure. The vertical dotted line represents the rising point of the BOLD signal. BOLD signals from contralateral non-activated regions are also displayed in the last row.

After the fMRI investigation, the patient received a new antiepileptic drug regime (a

combination of 1800 mg valproic acid, 225 mg topiramate, and 600 mg ethosuximide) and now she has only one seizure per month. Thus, no epilepsy surgery or further presurgical evaluation was performed.

3.4.2. Discussion

Only a few ictal fMRI studies have been presented in the literature so far (Jackson et al, 1994; Detre et al, 1995; Detre et al, 1996; Kubota et al, 2000; Krings et al, 2000; Federico et al, 2005; Salek-Haddadi et al, 2002; Kobayashi et al, 2006). Despite the advantage of high spatial resolution, ictal fMRI is only applicable to epilepsy patients under special circumstances: frequent seizures, preserved consciousness, no rough ictal movements.

To the best of our knowledge, our study is the first in the literature that visualizes the seizure onset zone and spread of a clinical seizure in epilepsy without detectable epileptogenic lesion. The seizure spread included diverse subcortical and cortical activations (Figure 19) that would provide new insight into the pathophysiology of seizure spread. Further, an anatomical region showing the first activation was determined, thus guidance for invasive examinations is possible to identify the putative seizure onset zone. It was especially important because the patient had already undergone two unsuccessful surgeries on the basis of invasive electrophysiological findings. However, it is obvious that more ictal fMRI examinations would be necessary to prove the uniformity of the seizure onset.

Previous ictal fMRI studies were mostly carried out on patients with known epileptogenic lesions including Rassmussen's encephalitis (Jackson et al, 1994), chronic gliosis (Detre et al, 1995; Detre et al, 1996), brain tumors (Kubota et al, 2000; Krings et al, 2000) or gray matter nodular heterotopia (Kobayashi et al, 2006). Moreover, no subcortical activation was observed in these studies except for a study conducted by Detre and coworkers (Detre

et al, 1996). However, no overt seizure was reported during the examination that questions the real background of the BOLD signal change (Detre et al, 1996). A recent EEG-fMRI study of a subclinical EEG seizure (Salek-Haddadi et al, 2002) tried to analyze the seizure spread, however the BOLD signal alteration lasted only for several seconds with a percent change of 2.5%.

It appears that, similar to the present study, BOLD signal shows a regular peak over minutes in clinically detectable seizures and a relative signal change of 4-9% (Jackson et al, 1994; Kubota et al, 2000; Krings et al, 2000). This means that presumably a much stronger haemodynamic response is present in manifest seizure than those observed during interictal activity or in standard motor/visual/cognitive paradigms. Further, the analysis of ictal data is hampered by the fact that no model haemodynamic response function is known in seizure. This is the reason why an internal reference function was chosen that is similar to those "ictal" BOLD responses published in the literature. The "ictal" BOLD response appears to have a bell-shaped form without obvious plateau (Jackson et al, 1994; Kubota et al, 2000; Krings et al, 2000) that is observed in the repetitive motor/visual or cognitive paradigms.

The application of low magnetic field for ictal fMRI in the present study was necessary due to the susceptibility artifacts occurred near the operated brain areas. The observed BOLD signal change of 9% well within the range of other studies performed at higher field strength. It also supports the observation that BOLD signal changes at low and high magnetic field can be comparable, if the measuring parameters and post-processing are optimized (Lundervold et al, 1995; Santosh et al, 1995).

The post-processing of ictal fMRI data shows a large diversity in the literature including image subtraction (Jackson et al, 1994), signal percent change images (Detre et al, 1995; Krings et al, 2000), cross-correlation (Detre et al, 1996; Kubota et al, 2000), t-test or F-test

using model hemodynamic functions (Salek-Haddadi et al, 2002; Kobayashi et al, 2006). Beside color-coded images in the papers, only a few BOLD signal changes are displayed originating from 1-3 volume of interests. In our study it was substantial that several BOLD signal change should be demonstrated reflecting the reliability of the applied post-processing technique (Figure 19).

We localized (i) the lower anterior part of the insular cortex as a seizure onset zone for epileptic activity, (ii) the motor cortex responsible for the mouth clonus and (iii) numerous other areas acting in the epileptic network. Interestingly, activation was found in left (ie. ipsilateral to the involved motor cortex) cerebellar hemisphere, but no activation was found in the right (Figures 18, 19), though it was expected (Van Paeschen 2004). However, Blumfeld and coworkers have found significant positive correlation in the ipsilateral medial cerebellar cortex in their SPECT study (Blumenfeld et al, 2004).

According to our findings, there is type of seizure spread that can be measured in seconds to minutes which is in agreement with intracranial studies (Lieb et al, 1991; Kim et al, 2004). Although, antero-posterior and baso-apical tendency in the spread can be noticed, the activation did not seem to spread in radial direction at a time resolution of 2.5 s, suggesting complex connection between the structures. For example, there is about one and half minute delay between the activation of the lower and the upper part of the insular cortex suggesting that either there is a blockage within the insular cortex and the activation comes via another structures, or somehow, the activation spread is slower within the insular cortex. Conversely, a seizure spread shorter than 2.5s cannot be detected by the present method which is one of the limitations of our study.

Our results also support the existence of the pre-ictal state that can vary from seconds to minutes (Federico et al, 2005; Baumgartner and Aull-Watschinger 2005). Although, the motor cortex responsible for mouth cloni during the seizure showed only 7.5 second long

pre-ictal phase, the activation in the lower part of the insular cortex occurred 80 seconds before the clinical seizure onset. In addition, some regions became activated after the clinical onset, supposing a post-ictal activation. Of course assuming that the BOLD signal changes are usually delayed by several seconds in comparison to neuronal activity changes the real pre-ictal phase may be several seconds longer than the recorded pre-ictal phase, according to the delay.

Limitations

It should be noted that no simultaneous EEG-fMRI was performed which would have helped in determining of the seizure onset zone. Thus, there is no direct evidence that all regions with BOLD response (i.e. haemodynamic change) are involved in the evolution of the seizure. However, the magnitude of the BOLD signal (4-8%) indicates that the haemodynamic response is much stronger than those usually seen in motor, visual, or cognitive paradigms (i.e. 2-4%). The other limitation of the study originates from the analysis: the use of an internal reference curve may exclude other BOLD responses that last considerably longer or shorter. However, a BOLD response in clinically detectable seizures lasts for minutes according to literature data (Jackson et al, 1994; Kubota et al, 2000; Krings et al, 2000). The other uncertainty is the detection of precise timing in the activation of a particular area. It is obvious from Figure 19 that in several areas there is gradual monotonous signal increase similar to those found in the pre-ictal state (Federico et al, 2005). So the determination of the rising point of a gradually increasing BOLD signal can be subjective.

3.5. Combining with DTI-FT

3.5.1. Results

Anatomical and functional MR examination

It is clearly visible on T_2-weighted anatomical images (Figure 7) that damages caused by TBI are the most severe on the left hemisphere. As other signs of damages, pathological signal alteration can be observed bilaterally in the cortical, subcortical regions and in the brain stem.

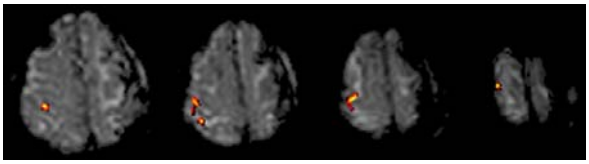

Figure 20. *FMRI with bilateral PFM of the patient.* Activations are illustrated with red-yellow colormap.

Evaluation of fMRI dataset resulted correlation coefficients of 0.175 and 0.459 referring to the lower (p = 0.05) and upper (p = 0.001) thresholds. Bilateral PFM resulted no activation on the left – where damages were greater –; while on right, activation of the pre- and postcentral gyri are visible (Figure 20).

DTI-FT

Examination lasted 25 minutes and resulted 6936 images ((16 (directions) + 1 (T_2-weighted)) x 34 (slices) x 12 (repetitions)).

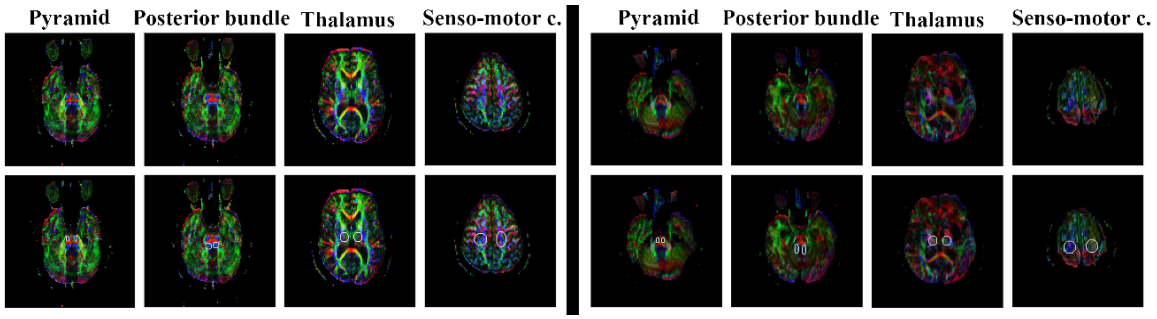

Figure 21. *Colorcoded DTI-maps of a healthy volunteer (left side) and the patient (right side) without (upper) and with (lower) ROI.* Cranio-caudal, antero-posterior and medio-lateral fibers are marked with blue, green and red respectively.

Colorcoded DTI-maps (Figure 21) shows craniocaudal fibres – marked with blue – in most slices, according to the location of the pyramidal tract. On the images of the healthy

volunteer (left side of Figure 21), these regions are more clearly separated; while on those of the patient (right side of Figure 21), these regions are located more inordinately.

Similar results were provided by FT (Figure 22) and the statistical analysis of the fibers (Table 4). In both subjects, fibers were visualized in the supposed location of the pyramidal tract, the posterior bundle, the thalamo-cortical tract and the ponto-cerebelar tract. The properties of the fibers were different, though. In healthy subject, pyramidal tract were able to be demonstrated in its whole length (left side of Figure 22) using any ROI. In contrary, in the patient, we could not observe the whole pyramidal tract using any ROI (right side of Figure 22): In case of ROI in the upper slices, some fragments are visible, but in the basal slices only the ponto-cerebellar and some fibers belonging to the posterior bundle are present.

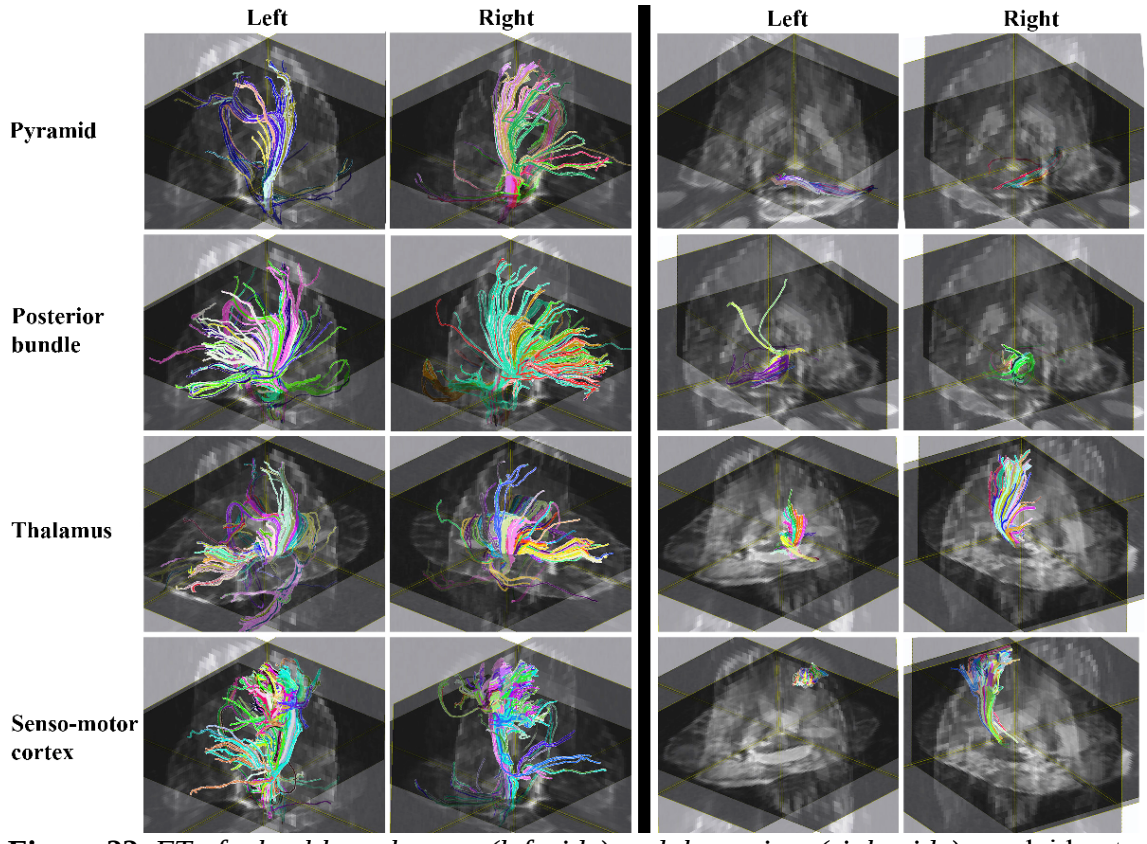

Figure 22. *FT of a healthy volunteer (left side) and the patient (right side)* overlaid onto the T_2-wighted images. Each fiber is marked with different colors. Point of view is the convexity of the frontal cortex on the marked side (left or right).

Table 4. Statistical analysis of fibers					
	ROI	**ROI area (pixel)**	**No. of fibers**	**Density of fibers (no./pixel)**	**Mean fiber length (mm)**
Healthy subject	*Whole brain*		***69617***		***43,32***
	Pyramid Left	15	190	12,67	116,26
	Pyramid Right	15	254	16,93	123,71
	Posterior bundle Left	32	494	15,44	93,29
	Posterior bundle Right	32	566	17,69	94,70
	Thalamus Left	60	371	6,18	84,04
	Thalamus Right	60	159	2,65	68,68
	Senso-motor c. Left	115	1100	9,57	69,55
	Senso-motor c. Right	116	984	8,48	67,23
	Mean (ROI) Left		*538,75*	*10,96*	*90,79*
	Mean (ROI) Right		*490,75*	*11,44*	*88,58*
	R-L Difference (%)		*-8,91*	*4,33*	***-2,43***
	Mean (ROI)		*514,75*	***11,20***	***89,68***
Patient	*Whole brain*		***36552***		***27,26***
	Pyramid Left	15	62	4,13	48,82
	Pyramid Right	15	40	2,67	66,16
	Posterior bundle Left	32	98	3,06	47,25
	Posterior bundle Right	32	70	2,19	33,74
	Thalamus Left	60	201	3,35	30,61
	Thalamus Right	60	269	4,48	61,34
	Senso-motor c. Left	116	175	1,51	20,06
	Senso-motor c. Right	116	343	2,96	40,10
	Mean (ROI) Left		*134,00*	*3,01*	*36,68*
	Mean (ROI) Right		*180,50*	*3,07*	*50,34*
	R-L Difference (%)		*34,70*	*1,99*	***37,21***
	Mean (ROI)		*157,25*	***3,04***	***43,51***

Statistical analysis provided similar result. Less fiber were observed in the patient taking account fiber either in the whole brain (healthy subject: 69617; patient: 36552) or just in the ROIs (mean density: healthy subject: 11.2 fibers/pixel; patient: 3.04 fibers/pixel); moreover, fibers were observed to be shorter (mean length: healthy subject: 43.32 mm; patient: 27.26 mm), as those in healthy subject. Difference is much pronounced taking account fibers just in the ROIs (mean length: healthy subject: 89.68 mm; patient: 43.51 mm) as selecting mostly the long tracts. In patient, a left-right difference can be also noticed: fibers on the right are longer with 37.21% than those on the left. E.g. thalamo-cortical tract is fragmented more severely on the left. There are two exceptions: second row on the right side of Figure 22 demonstrates a long fiber coming through the ROI on the left and running to the right cortex; and ponto-cerebelar tract also seems to be intact

just on the left. In case of healthy subject, no such difference can be noticed (-2.43%).

3.5.2. Discussion

FMRI

Examination could visualize the senso-motor cortex with good quality and resolution. In the central region, activity can be observed just on the right side with less damage; however, PFM was conducted bilaterally. Absence of activation could be due to either damage of the cortex or discontinuity of fibers running to the cortex.

DTI-FT

Based on the results of two measurements, we can conclude that we could visualize damages of fibers caused by TBI with good quality and resolution. Examination and evaluation of healthy subject can demonstrate the pyramidal tract, the posterior bundle, the ponto-cerebellar tract, the fronto-pontin tract, the thalamo-cortical system, and other associational, commissural and projecting fibers with quality close to anatomy.

Our results support those from routine diagnostics, too. Distribution of the damages of fibers is in good concordance with the mechanism of the injury: As trauma had come from the left-front, fibers located there (fibers running through ROIs on the left, especially frontal part of thalamo-cortical fibers) damaged more severely. Posterior bundle crossing partially (second row on the right side of Figure 22) seems to be an exception. However, only fibers running to the right hemisphere are demonstrated. No fibers running through ROI on the right to the ipsilateral (right) hemisphere were visualized referring to a pronounced damage of the right-posterior part of the brain stem, as a result from the “coup-contrecoup” injury caused by the acceleration-deceleration mechanism. It also explains why the damage in the cerebellum is more severe on the right.

Results from DTI-FT can also help to explain that of fMRI. We could find intact crossing fiber belonging to the posterior bundle only in the right hemisphere able to pass information from the patient's left hand to the right senso-motor cortex.

These results show the level of the damages, too. Beside the injured cortex and subcortical white matter, subcortical connections – especially below the level of the thalamus – were severely impaired.

Limits of DTI-FT

Method of FT has limits causing problems at both high and low field. (1) Some pathology greatly hampers the analysis. In case of e.g. edema the relative amount water molecules with isotropic diffusion increases causing lower FA. In such a voxel, tracking of the fiber stops. We can try setting the FA-threshold to lower, however, resulting in more false positive fibers. (2) Setting thresholds is quite subjective. Because of few experience and high individual variability, there is no standard guide to determine these thresholds (especially in case like (1)). Moreover, programs for DTI-analysis apply different approach (absolute signal intensity, length of fiber etc.) to determine conditions of FT. (3) Fiber-crossing is an other issue. As voxel-size is much bigger than size of fibers, there are surely voxels containing fibers with different directionality. However, evaluation selects only one direction for each voxel impeding FT in the other directions. Its effect can be minimized decreasing voxel-size, however, just to a certain extent; because we cannot achieve voxel-size of several μm. The other possible workaround may be using such an approach for evaluation that takes this phenomenon into account.

The greatest disadvantage caused by low field is the longer examination time. Due to the lower SNR, more repetitions are necessary. Besides with proper settings results seems appropriate enough in comparison with those obtained at e.g. 1.5 T (Yu et al, 2005).

4. Recording neural activities by means of SPECT using modified SISCOM-analysis

4.1. Results

The appearance of DV

Preoperatively the patient had never experienced any DVs. Immediately after turning on the *DV-inducing stimulation*, an unusual and obscure feeling appeared. Besides discomfort and slight disturbance, the subject had intact reality sense; she was able to observe what is going on around her and maintain verbal and behavioral responsiveness. We defined this experience as 'standby-state for DV (SSDV)'. The SSDV persisted until the stimulation of contact 0 was turned off or the amplitude of stimulation was lowered below 2.7 Volts. We tested several times the turning on or off the stimulation of contact 0 and decreasing or increasing the stimulation voltage across the threshold-level; but the patient always adequately indicated the presence or absence of SSDV without exception.

During SSDV, sudden, impulse DV experiences appeared lasting 4-5 seconds. At these occasions she felt that the situation seemed familiar. No visual, auditory illusions or hallucinations accompanied the DV. Besides, the patient felt neither the ability to predict the future nor unreality about the current circumstances.

DV appeared more frequent immediately after turning the stimulation on (approximately 2-5 DV during the first 5-10 minutes) and became rarer as the time went by (approximately another 3-5 DV in the first hour and 2-3 in the second hour). Interestingly, DV appeared only if her eyes were open and questions were addressed directly to the patient (e.g. "What is the name of your physiotherapist?"). However, not all of the direct questioning of the patient elicited DV. Standard digital EEG recording showed physiologic activity and there were no clinical signs of epilepsy either.

MRI

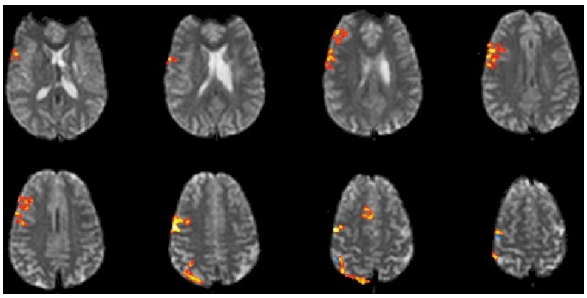

Figure 23. *FMRI with IWG of the patient.*

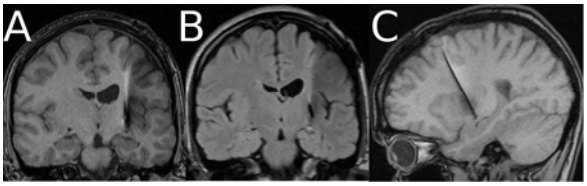

Figure 24. *The postoperative MR.*
(A) coronal MP-RAGE, (B) coronal FLAIR
(C) sagittal MP-RAGE

Preoperative fMRI demonstrated right-sided language dominance (Figure 23). The postoperative MRI demonstrated that the stimulating electrode passed through the GPi, which was confirmed by the fact that the normal stimulation decreased the severity of dystonia. Visual inspection and the application of electronic version of stereotactic atlas (Schaltenbrand and Wahren, 1977) verified that this contact was situated between the GPi and the underlying white matter (Figure 24). The electrode did not hit the mesial temporal structures. The exact position of the lowest contact, whose stimulation could elicit DV, was the following: 22 mm lateral from the midline, 13 mm anterior to the posterior commissure, 12 mm bellow the intercommissural line (the distance between the anterior and posterior commissure was 24.9 mm).

SPECT

The results of SISCOM analysis are demonstrated on Figure 25. Compared to the baseline, SPECT during DV showed *right-sided hyperperfusion* of hippocampus, parahippocampal gyrus, fusiform gyrus, cerebellum and temporal

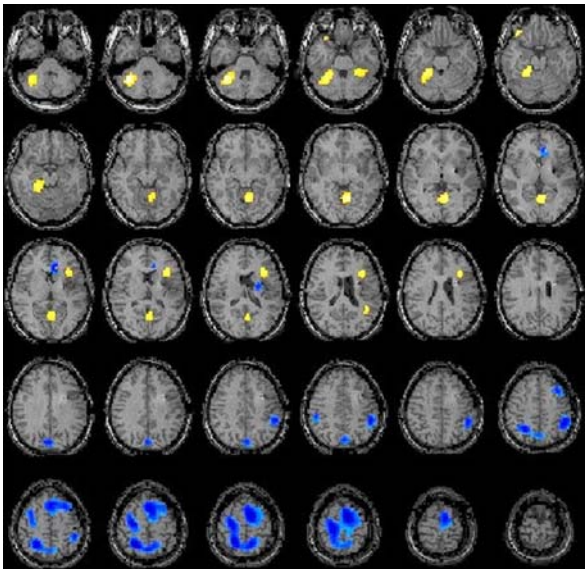

Figure 25. *SISCOM analysis.*
yellow: hyperperfusion, blue: hypoperfusion

superior pole; *left-sided hyperperfusion* appeared in the cerebellum, operculum, insula, lingual gyrus, precuneus and middle temporal gyrus. *Hypoperfusion* appeared bilaterally in the precentral and postcentral gyri, as well as, in the frontal (especially supplementary motor cortex) and parietal areas.

4.2. Discussion

In our patient the electrically evoked déjà vu phenomenon could be easily studied because of several reasons: (1) it could be repeated without any restraints; (2) déjà vu could be elicited for a controlled period; (3) no other neurological phenomenon disturbed the evaluation; (4) the examinations did not bother or harm the patient.

Clinical manifestation

A surprising finding was that during pallidal stimulation two distinct types of symptoms occurred: SSDV and DV. SSDV was elicited merely by the stimulation, while DV phenomena appeared only in SSDV and when the patient's eyes were open and she was addressed with direct questions indicating that certain level of arousal and/or visual stimuli were needed for DV. The occurrence of DV seemed to have a habituating feature, i.e. in the first 5 minutes after starting the stimulation of contact 0 produced more frequent DV appearance (2-5 during the first 5 minutes), which became rarer with time. Although DV was a transitory experience lasting for a few seconds, on the 'ictal' SPECT scan we could identify the brain structures involved in DV, since the patient experienced several DVs during the interval of tracer binding. Therefore, the subtraction of 'ictal' and 'baseline' images presumably corresponds to only those areas responsible for both type of DV.

Neuroanatomical considerations

Based on the position of the stimulation electrode, we might speculate the anatomical target responsible for DV. The postoperative MRI scans demonstrated that contact 0 was situated in the border of GPi and the underlying white matter. The spreading of electrical current is roughly spherical around the activated contact and in no case extends underneath the electrode (Buston et al, 2007). We can also presume that the electricity can diffuse approximately up to 4 millimeters in a low impedance tissue from the surface of the contact (Butson, Maks and McIntyre, 2006). Therefore, the anatomical structures or pathways responsible for DV were probably located up to 4 mm around contact 0 and the direct stimulation of mesiotemporal structures was unlikely.

We performed subtraction SPECT analysis comparing 'ictal' and 'baseline' SPECT images. The subtracted picture revealed hyperperfusion in the right mesial structures contralateral to the stimulation. There was also hyperperfusion of ipsilateral (left) operculum, insula, precuneus and lingual gyrus. This finding is in harmony with TLE studies (Bancaud et al, 1994) demonstrating that the elicitation of DV involves mainly mesiotemporal structures.

Proposed theories on pathophysiology on DV

As far as the authors are aware, there is not even a single case published describing the occurrence of déjà vu after pallidotomies, despite several ten thousands were performed worldwide (Gross et al, 1999; Guridi and Lozano, 1997). Because ablative procedures could not evoke DVs and certain stimulation settings were required to produce DV, we may presume the importance of high-frequency stimulation in the background.

(1) We can hypothesize that ***several independent constellations*** together led to DV: (i) the SSDV and a certain combination of (ii) visual and (iii) direct verbal stimuli requiring

memory matching processes. This hypothesis is based on the fact that the DV-inducing stimulation itself was unable to produce DV in the lack of simultaneous visual and verbal stimuli; it elicited "only" the SSDV. Clinically, DV appeared only when the patient was addressed with questions and her eyes were open. The type of visual stimuli seemed to be irrelevant in the elicitation, because DV appeared in both dim and bright rooms, either with or without persons in the visual field. On the contrary, only direct questioning of the patient was able to elicit DV, other auditory stimuli (e.g. environmental noises, conversation between other persons not involving the patient) never did so. However, not all questioning elicited DV. One potential explanation for this phenomenon might be that direct questioning requires high-level attention, interpretation and memory processing.

(2) Probably not only the left GPi stimulation itself, but also the ***individual (atypical) neuroanatomy*** might play a role in the development of DV. The atypical language dominance suggests that due to the perinatal brain injury our patient developed an atypical brain anatomy (Jacola et al, 2006; Janszky et al, 2003; Muller et al, 1998; Rasmussen and Milner, 1977). Because the reorganization of the injured brain is not always complete, similar modalities might be present bilaterally and the division of labor between dominant and non-dominant hemisphere functions might not be completed. Normally, language-dominant hemisphere is more strongly engaged in memory processing of verbal material (Weber et al, 2007). However, in our case the individual neuroanatomy might have produced that non-verbal functions are confined to both hemispheres. If this speculation is true, the disturbing effect of left GPi DBS might have greater impact on one hemisphere and less on the other one producing DV. The elicitation of DV seemed to be a habituating phenomenon. An explanation for this habituation may be that the memory processing system(s) noticed the DVs as errors. Possibly, this error recognition enabled the system to adapt to the SSDV resulting in less DV experiences over time.

(3) The **non-dominant localization of the GPi stimulating electrode** might have also had an impact on DV-elicitation. Previous electrophysiological studies confined the DV to the non-dominant hemisphere. However, these studies were limited to the TLE (Bancaud et al, 1994; Gloor, 1982).

Open questions

Several questions remain unanswered in our case. We only compared the functional neuroimages between the *DV-eliciting* and the "normal" pallidal stimulation. Because during the interval of tracer binding four déjà vu episodes occurred, the difference of these scans supposedly identifies the anatomical structures responsible for DV. However, we should have obtained a third SPECT scan during SSDV without DV during tracer binding to compare the different activations between the DV and SSDV and between the SSDV and the normal stimulation. This way, we could have identified those structures, which are directly responsible for the DV experience but does not contribute to the SSDV. Respecting the request of our patient, we have forborne from this acquisition.

5. Conclusions

5.1. Recording neural activities by means of MRI at low magnetic field

5.1.1. Optimizing parameters at low magnetic field

In conclusion, adequate post-processing allows for functional MRI of human brain activation on a routine clinical instrument even at a low magnetic field strength of 1 T. The approach is feasible, sensitive, and – compared with data obtained at 3 T – reliable. This observation is in accordance with the few published studies performed at 1 T (Jones et al, 1998; Van Borsel et al, 2003; Lundervold et al, 1995; Santosh, Rimmington and Best, 1995; Hoogenraad et al, 1998). Similar functional contrast, i.e., MRI signal changes in response to a functional challenge, may be obtained at different field strengths by adjusting the gradient echo time, while keeping the spatial resolution constant. The use of a suitable post-processing strategy may largely compensate for low SNR.

5.1.2. Diagnostic studies (neurosurgical planning and functional neuronavigation)

FMRI as a part of routine neurosurgical evaluation has been set up for a long time in abroad. In Hungary, we was the first who uses it in a clinical routine; and 114 sessions with 48 patients examined and operated based on the results surely prove, that (a) fMRI of clinically relevant paradigms with proper settings is easy to use, (b) it can be acquired and analyzed with good quality even at 1T (c) visualizing the eloquent areas with good accuracy, and (d) able to be applied for neurosurgical planning and functional neuronavigation. It can provide accurate and flexible real-time functional guidance for the neurosurgeon making other invasive and cost- and resource-demanding methods unnecessary. (e) Finally, as we accomplished the examinations on a clinical scanner widely available in Hungary; this method can be widely applied.

5.1.3. A novel group analysis

The proposed TTC group analysis for fMRI appears to be advantageous in several respects: (a) it is simple, transparent, and fast, (b) it is robust with respect to physiologic variability by estimating the noise distribution and respective thresholds from the actual experiment, and (c) it may minimize the problem of false positive activations by combining two thresholds for the identification of activations and by taking the mean of individual CC values for the respective group analysis.

5.1.4. Visualizing epileptic activity

To our knowledge, ours is the first study that describes, simultaneously in time and space, whole-brain haemodynamic changes during an epileptic seizure. Our observations might contribute to a better understanding of the pathophysiology of seizure spread. Moreover, the identification of the putative seizure-onset zone can be crucial for presurgical evaluation of epilepsy patients. In the case presented, the putative seizure-onset zone could have been validated by successful surgery. However, the frequency and severity of the patient's seizures have been considerably reduced, and she refused to undergo further invasive investigations.

5.1.5. Combining with DTI-FT

DTI-FT even at low field can *in vivo* visualize neural tracts adequately mirroring their actual position and status thus improving the diagnosis of e.g. TBI. It is important to notice, that our application is just one of the many possible ones. This method can provide useful information about other pathologies affecting white matter (brain tumor, multiple sclerosis, dyslexia, schizophrenia etc.). Finally, as we accomplished the examinations on a clinical scanner widely available in Hungary; this method can be widely applied.

5.2. Recording neural activities by means of SPECT using modified SISCOM-analysis

To our knowledge, ours is the first study that describes, simultaneously in time and space, whole-brain hemodynamic changes during DV. Our observation is in good concordance with those in literature. Summing up our results and theories with those of others, we may assume that certain constellation (e.g. DBS wit specific electrode localizations and stimulation parameters, individual neuroanatomy and certain cognitive state) is needed to be able to elicit DV.

6. Application of novel functional imaging techniques at low magnetic field in routine clinical work and neuroscience

Novel neuroimaging techniques can *in vivo* visualize function and structure of human nervous system. The advantages of fMRI in comparison with other functional neuroimaging methods especially PET and SPECT are that this technique includes, in addition to their multiplanar imaging ability, low invasiveness and lack of radiation; furthermore fMRI has a far better resolution in time and space. Moreover, the costs of fMRI are lower and can be easy used even in standard hospital environment. These advantages are the main causes why fMRI become the most used functional neuroimaging method nowadays. Functional MR imaging techniques have also revolutionized the study of neurological illness. In several diseases, these imaging techniques can improve early detection, characterization; and selecting, planning, monitoring and intensifying of therapy. Due to the easy manageability and low invasiveness, fMRI is far the most popular functional neuroimaging technique in neuroscience. In contrary with other methods (e.g. PET, SPECT) fMRI can be applied almost without restrictions: examinations can be repeated and extended to more subjects – even to children. Initial results have already provided insight into the pathophysiological changes of different diseases especially in reorganization of normal human brain functions after neural injury. In more studies, authors could detect traits marking both disposition to different diseases and responsiveness to different therapies, which may make diagnosis and therapy more efficient.

Besides clinical research, with FMRI we can obtain insight into our brain and cognition. We can determine structures or better to say networks responsible for various behavior and mental processes; and – with the help of neurofeedback (Weiskopf et al, 2007) – we can even train them to restore or improve their performance.

In the recent years this technique has become possible also in Hungary including our center where the most important fMRI techniques in clinical neurology and neurosurgery as well as in neuroscientific research can be routinely used. As my thesis demonstrates, these techniques can be accomplished even at low field with great success with proper settings of acquisition parameters and appropriate post-processing methods. Even for those who have access only to low-field MRI systems, there could be a wider spectrum of diagnostic possibilities and useful scientific methods at hand.

There is no "ultimate" tool, however, and fMRI also has its own limitations; but considering them we can choose an ideal tool or combine it with others thus providing answer for our actual question.

"Success is not the key to happiness. Happiness is the key to success. If you love what you are doing, you will be successful."

(Albert Schweizer)

7. References

Albers GW, Lansberg MG, Norbash AM, Tong DC, O'Brien MW, Woolfenden AR, et al. Yield of diffusionweighted MRI for detection of potentially relevant findings in stroke patients. Neurology 2000;54:1562-7.

Andersen AR. 99mTc-D,L-hexamethylene-propyleneamine oxime (99mTc-HMPAO): basic kinetic studies of a tracer of cerebral blood flow. Cerebrovasc Brain Metab Rev 1989;1:288-318.

Azmi H, Biswal B, Salas S, Schulder M. Functional imaging in a low-field, mobile intraoperative magnetic resonance scanner: expanded paradigms. Neurosurgery 2007;60:143-148.

Baird AE, Warach S. Magnetic resonance imaging of acute stroke. J Cerebr Blood Flow Metabo 1998;18:583-609.

Bancaud J, Brunet-Bourgin F, Chauvel P, Halgren E. Anatomical origin of deja vu and vivid 'memories' in human temporal lobe epilepsy. Brain 1994;117:71-90.

Baraldi P, Porro CA, Serafini M, Pagnoni G, Murari C, Corazza R, Nichelli P. Bilateral representation of sequential finger movements in human cortical areas. Neurosci Lett 1999;269:95-98.

Basser PJ, Mattiello J, Le Bihan D. MR diffusion tensor spectroscopy and imaging. Biophys J 1994;66:259-67.

Basser PJ, Jones DK. Diffusion-tensor MRI: theory, experimental design, and data analysis. NMR Biomed 2002;15:456-7.

Baudewig J, Dechent P, Merboldt KD, Frahm J. Thresholding in correlation analyses of magnetic resonance functional neuroimaging. Magn Reson Imaging 2003;21:1121-30.

Baumgartner C, Aull-Watschinger. The preictal state in focal epilepsy. Lancet 2005;366:2065-2066.

Belliveau JW, Kennedy DN, MCKinistry RC et al. Functional mapping of the human visual cortex by magnetic resonance imaging. Science 1991;254:716-19.

Bloch F, Hansen WW, Packard M. "Nuclear induction". Phys Rev 1946;69:127.

Blumenfeld H, McNally KA, Vanderhill SD, Paige AL, Chung R, Davis K, Norden AD, Stokking R, Studholme C, Novotny EJ Jr, Zubal IG, Spencer SS. Positive and negative network correlations in temporal lobe epilepsy. Cerebral Cortex 2004;14:892-902.

Butson CR, Maks CB, McIntyre CC. Sources and effects of electrode impedance during deep brain stimulation. Clin Neurophysiol 2006;117:447-54.

Butson CR, Cooper SE, Henderson JM, McIntyre CC. Patient-specific analysis of the volume of tissue activated during deep brain stimulation. Neuroimage 2007; 34:661-70.

Chenevert TL, Brunberg JA, Pipe JG. Anisotropic diffusion within human white matter: demonstration with NMR technique in vivo. Radiology 1990;177:401-5.

Collins L. 3D Model-based segmentation of individual brain structures from magnetic resonance imaging data. Thesis, McGill Univ, Canada 1994.

Damadian R, Minkoff L, Goldsmith M, Koutcher JA. Field-focusing nuclear nuclear magnetic resonance (fomar). Naturwissenschaften 1978;65:250-2.

Detre JA, Sirven JI, Alsop DC, et al. Localization of subclinical ictal activity by functional magnetic resonance imaging: Correlation with invasive monitoring. Ann Neurol 1995;44:850-6.

Detre JA, Alsop DC, Aguirre GK, et al. Coupling of cortical and thalamic ictal activity in human partial epilepsy: demonstration by functional magnetic resonance imaging. Epilepsia 1996;37:657-61.

Deutsch GK, Dougherty RF, Bammer R, Siok WT, Gabrieli JD, Wandell B. Children's reading performance is correlated with white matter structure measured by diffusion tensor imaging. Cortex 2005;41:354-63.

Douek P, Turner R, Pekar J, Patronas NJ, Le Bihan DJ. MR color mapping of myelin fiber orientation. J Comput Assist Tomogr 1991;15:923-9.

Engel J, Dichter MA, Schwartzkroin PA. Basic mechanisms in human epilepsy. In: Engel J, Pedley TA, eds. Epilepsy-a comprehensive textbook. 2nd edition. Philadelphia: Wolters luwer Health/Lippincot-Williams and Wilkins, 2007:495-505.

Federico P, Abbott DF, Briellmann RS, et al. Functional MRI of the pre-ictal state. Brain 2005;128:1811-7.

Fera F, Yongbi MN, van Gelderen P, Frank JA, Mattay VS, Duyn JH. EPI-BOLD fMRI of human motor cortex at 1.5 T and 3.0 T: sensitivity dependence on echo time and acquisition bandwidth. J Magn Reson Imaging 2004;19:19-26.

Fischl B, Van der Kouwe A, Destrieux C, et al. Automatically parcellating the human cerebral cortex. Cereb Cortex 2004;14:11-22.

Fox PT, Minutun MA, Raichle ME, Herscovitch P. A noninvasive approach to quantitative functional brain maping with H2 (15)O and positron emission tomography. J Cerebr Blood Flow Metab 1984;4:329-33.

Fox PT, Raichle ME. Focal physiological uncoupling of cerebral blood flow and oxidative metabolism during somatosensory stimulation in human subject. Proc Natl Acad Sci USA 1986;83:1140-44.

Friston KJ, Holmes AP, Worsley KP, Poline JP, Frith CD, Frackowiak RSJ. Statistical parametric maps in functional imaging: a general linear approach. Hum Brain Map 1995;2:189-210.

Gati JS, Menon RS, Ugurbil K, Rutt BK. Experimental determination of the BOLD field strength dependence in vessels and tissue. Magn Reson Med 1997;38:296-302.

Genovese CR, Lazar NA, Nichols T. Thresholding of Statistical Maps in Functional Neuroimaging Using the False Discovery Rate. NeuroImage 2002;15:870-8.

Gering DT, Weber DM. Intraoperative, real-time, functional MRI. J Magn Reson Imaging 1998;8:254-257.

Gloor P, Olivier A, Quesney LF, Andermann F, Horowitz S. The role of the limbic system in experiential phenomena of temporal lobe epilepsy. Ann Neurol 1982;12:129-144.

Gotman J, Grova C, Bagshaw A, Kobayashi E, Aghakhani Y, Dubeau F. Generalized epileptic discharges show thalamocortical activation and suspension of the default state of the brain. Proc Natl Acad Sci USA 2005;102:15236-40.

Gross CE, Boraud T, Guehl D, Bioulac B, Bezard E. From experimentation to the surgical treatment of Parkinson's disease: prelude or suite in basal ganglia research? Prog Neurobiol 1999;59:509-532.

Guridi J, Lozano AM. A brief history of pallidotomy. Neurosurgery 1997;41:1169-1180.

Haase A, Frahm J, Matthaei D, Hänicke W, Merboldt KD. FLASH imaging: rapid NMR imaging using low flip angle pulses. J Magn Res 1986;67:258-266.

Haase L, Cerf-Ducastel B, Buracas G, Murphy C. On-line psychophysical data acquisition and event-related fMRI protocol optimized for the investigation of brain activation in response to gustatory stimuli. J Neurosci Methods. 2007;159:98-107.

Hajnal JV, Collins AG, White SJ, Pennock JM, Oatridge A, Baudouin CJ, Young IR, Bydder GM. Imaging of human brain activity at 0.15 T using fluid attenuated inversion recovery (FLAIR) pulse sequences. Magn Reson Med 1993;30:650-653.

Havel P, Braun B, Rau S, Tonn JC, Fesl G, Brückmann H, Ilmberger. Reproducibility of activation in four motor paradigms. An fMRI study. J Neurol 2006;253:471-476.

Hesseltine SM, Law M, Babb J, Rad M, Lopez S, Ge Y, et al. Diffusion tensor imaging in multiple sclerosis: assessment of regional differences in the axial plane within normal-appearing cervical spinal cord. Am J Neuroradiol 2006;27:1189-93.

Hollo A, Kaminska A, Vera P, et al. Ictal perfusion changes during occipital lobe seizures in infancy: report of two serial ictal observations. Epilepsia 2001;42:257-9.

Holloway V, Gadian DG, Vargha-Khadem F, Porter DA, Boyd SG, Connelly A. The reorganization of sensorimotor function in children after hemispherectomy: A functional MRI and somatosensory evoked potential study. Brain 2000;123:2432-44.

Hoogenraad FG, Reichenbach JR, Haacke EM, Lai S, Kuppusamy K, Sprenger M. In vivo measurement of changes in venous blood-oxygenation with high resolution functional MRI

at 0.95 tesla by measuring changes in susceptibility and velocity. Magn Reson Med 1998;39:97-107.

Huisman TA, Schwamm LH, Schaefer PW, Koroshetz WJ, Shetty-Alva N, Ozsunar Y, et al. Diffusion tensor imaging as potential biomarker of white matter injury in diffuse axonal injury. Am J Neuroradiol 2004;25:370-6.

Jackson JA, Langham WH. Whole-body NMR spectrometer. Rev Sci Instrum 39:510,1968.

Jackson GD, Connelly A, Cross JH, Gordon I, Gadian DG. Functional magnetic resonance imaging of focal seizures. Neurology 1994;44:850-856.

Jacola LM, Schapiro MB, Schmithorst VJ, Byars AW, Strawsburg RH, Szaflarski JP, Plante E, Holland SK. Functional magnetic resonance imaging reveals atypical language organization in children following perinatal left middle cerebral artery stroke. Neuropediatrics 2006;37:46-52.

Janszky J, Rásonyi G, Fogarasi A, et al. Műtéttel gyógyítható epilepszia – összefoglaló tanulmány. Orv Hetil 2001;142:1597-604.

Janszky J, Hollo A, Barsi P, et al. Misleading lateralization by ictal SPECT in temporal lobe epilepsy - a case report. Epileptic Disord 2002;4:159-62.

Janszky J, Jokeit H, Heinemann D, Schulz R, Woermann FG, Ebner A. Epileptic activity

influences the speech organisation in medial temporal lobe epilepsy. Brain 2003a;126:2043-51.

Janszky J, Ebner A, Kruse B, et al. The functional organization of the brain with malformations of cortical development Ann Neurol 2003b;53:759-67.

Janszky J, Ollech I, Jokeit H, Kontopoulou K, Mertens M, Pohlmann-Eden B, Ebner A, Woermann FG Epileptic activity influences the lateralization of mesiotemporal fMRI activity. Neurology 2004;63:1813-1817.

Janszky J, Janszky I, Schulz R, et al. Temporal lobe epilepsy with hippocampal sclerosis: predictors for long-term surgical outcome. Brain 2005a;128:395-404.

Janszky J, Jokeit H, Kontopoulou K, et al. Functional MRI predicts the memory performance after epilepsy surgery. Epilepsia 2005b;46:244-50.

Jokeit H, Okujava M, Woermann G. Memory fMRI lateralizes temporal lobe epilepsy. Neurology 2001;57:1786-93.

Jones AP, Hughes DG, Brettle DS, Robinson L, Sykes JR, Aziz Q, Hamdy S, Thompson DG, Derbyshire SW, Chen AC, Jones AK. Experiences with functional magnetic resonance imaging at 1 tesla. Br J Radiol 1998;71:160-166.

Kim SG, Ashe J, Hendrich K et al. Functional magnetic resonance imaging of motor cortex: Hemispheric asymmetry and handedness. Science 1993;261:615-17.

Kim OJ, Ahn JY, Lee BI. Analysis of electrical discharges made with the foramen ovale electrode recording technique in mesial temporal lobe epilepsy patients. Journal of Clinical Neurophysiology 2004;21:391-398.

Kleinschmidt A, Requardt M, Merboldt KD, Frahm J. On the use of temporal correlation coefficients for magnetic resonance mapping of functional brain activation. Individualized thresholds and spatial response delineation. Intern J Imag Sys Technol 1995;6:238-44.

Knowlton RC, Shih J. Magnetoencephalography in epilepsy. Epilepsia 2004;45(Suppl. 4):61-71.

Kobayashi E, Hawco CS, Grova C, et al.Widespread and intense BOLD changes during brief focal electrographic seizures. Neurology 2006;66:1049-55.

Koepp MJ, Richardson MP, Brooks DJ, et al. Focal cortical release of endogenous opioids during reading-induced seizures. Lancet 1998;352:952-5.

Kovacs N, Nagy F, Kover F, Feldmann A, Llumiguano C, Janszky J, Kotek Gy, Doczi T, Balas I. Implanted deep brain stimulator and 1.0-Tesla magnetic resonance imaging. J Magn Reson Imaging 2006;24:1409-12.

Krakow K, Woermann FG, Symms MR, et al. EEG-triggered functional MRI of interictal epileptiform activity in patients with partial seizures. Brain 1999;122:1679-88.

Krasnow B, Tamm L, Greicius MD, Yang TT, Glover GH, Reiss AL, Menon V. Comparison of fMRI activation at 3 and 1.5 T during perceptual, cognitive, and affective processing. Neuroimage 2003;18:813-826.

Krings T, Topper R, Reinges MH, et al. Hemodynamic changes in simple partial epilepsy: a functional MRI study. Neurology 2000;54:524-7.

Krüger G, Kastrup A, Glover GH. Neuroimaging at 1.5 T and 3.0 T: comparison of oxygenation-sensitive magnetic resonance imaging. Magn Reson Med 2001;45:595-604.

Kubota F, Kikuchi S, Ito M, et al. Ictal brain hemodynamics in the epileptic focus caused by a brain tumor using functional magnetic resonance imaging (fMRI). Seizure 2000;9:585-9.

Kumar A, Welti D, Ernst RR. "NMR Fourier zeugmatography." J Magn Reson 1975;18:69-83.

Lauterbur PC. Image formation by induced local interactions: examples employing nuclear magnetic resonance. Nature 1973;242:190.

Le Bihan D. Molecular diffusion, tissue microdynamics and microstructure. NMR Biomed 1995;8:375-86.

Le Bihan D, van Zijl PCM. From the diffusion coefficient to the diffusion tensor. NMR Biomed 2002;15:431-4.

Lezak MD. Neuropsychological assessment. New York: Oxford University Press; 1997.

Lieb JP, Dassheiff RM, Engel J. Role of the frontal lobes in the propagation of mesial temporal lobe seizures. Epilepsia 1991;32:822-837.

Lundervold A, Ersland L, Gjesdal KI, Smievoll AI, Tillung T, Sundberg H, Hugdahl K. Functional magnetic resonance imaging of primary visual processing using a 1.0 Tesla scanner. Int J Neurosci 1995;81:151-168.

Mansfield P. "Multi-planar image formation using NMR spin-echos." J Phys C: Solid State Physics 1977;10:55-58.

Merboldt KD, Fransson P, Bruhn H, Frahm J. Functional MRI of the human amygdala? Neuroimage 2001;14:253-257.

Molnár P. Az idegrendszer patológiája. In: Arató G, Balogh K, Bodó M, et al. Patológia. Budapest: Medicina Könyvkiadó; 2004. p.1277.

Mori S, Hangyi J, Kegang H. DTIStudio (http://lbam.med.jhmi.edu/DTIuser/DTIuser.asp)

Mori S, van Zijl PCM. Fiber tracking: principles and strategies. NMR Biomed 2002;15:468-80.

Moseley ME, Cohen Y, Kucharczyk J. Diffusion-weighted MRI imaging of anisotropic water diffusion in cat central nervous system. Radiology 1990;176:439-46.

Muller RA, Watson CE, Muzik O, Chakraborty PK, Chugani HT. Motor organization after early middle cerebral artery stroke: a PET study. Pediatr Neurol 1998;19:294-298.

Nichols T, Hayasaka S. Controlling the familywise error rate in functional neuroimaging: a comparative review. Stat Methods Med Res 2003;12:419-46.

O'Brien B, O'Connor M, Mullan BP. Subtraction ictal SPECT co-registered to MRI in partial epilepsy: description and technical validation of the method with phantom and patient studies. Nucl Med Commun 1998;19: 31-45.

Ogawa S, Lee TM, Kay AR, Tank DW. Brain magnetic resonance imaging with contrast dependent on blood oxygenation. Proc Natl Acad Sci USA 1990;87:9868-72.

Ogawa S, Tank DW, Menon R, Ellerman JM, Kim S-G, Merkle H. Intrinsic signal changes accompanying sensory stimulation: Functional brain mapping with magnetic resonance imaging. Proc Natl Acad Sci USA 1992;89:5952-5.

Oldfield RC. The assessment and analysis of handedness: the Edinburgh Inventory. Neuropsychologia 1971;9:97-113.

Pajevic S, Pierpaoli C. Color schemes to represent the orientation of anisotropic tissues from diffusion tensor data: application to white matter fiber tract mapping in the human brain. Magn Reson Med 1999;42:526-40.

Penfield W, Sántha K, Cipriani A. Cerebral blood flow during the induced epileptiform seizures in animals and man. J Neurophysiol 1939;2:257-67.

Pierpaoli C, Basser PJ. Toward a quantitative assessment of diffusion anisotropy. Magn Reson Med 1996;36:893-906.

Purcell EM, Torry HC, Pound CV. Resonance absorption by nuclear magnetic moments in a solid. Phys Rev 1946;69:37.

Rasmussen T, Milner B. The role of early left-brain injury in determining lateralization of cerebral speech functions. Ann N Y Acad Sci 1977;299:355-369.

Roy CS, Sherrington CS. On the regulation the blood supply of the brain. J Physiol (Lond) 1896;11:85-108.

Salek-Haddadi A, Merschhemke M, Lemieux L, et al. Simultaneous EEG-correlated ictal fMRI. Neuroimage 2002;16:32-40.

Salek-Haddadi A, Diehl B, Hamandi K, et al. Hemodynamic correlates of epileptiform discharges: an EEG-fMRI study of 63 patients with focal epilepsy. Brain Res 2006;1088:148-66.

Santosh CG, Rimmington JE, Best JJ. Functional magnetic resonance imaging at 1 T: motor cortex, supplementary motor area and visual cortex activation. Br J Radiol 1995;68:369-374.

Schaltenbrand G, Wahren B. Atlas for the sterotaxy of the human brain. Thieme, Stuttgart, Germany 1977.

Schlosser RG, Nenadic I, Wagner G, Gullmar D, von Consbruch K, Kohler S, et al. White matter abnormalities and brain activation in schizophrenia: A combined DTI and fMRI study. Schizophr Res 2007;89(1-3):1-11.

Schepers J, Schnell R, Vroom P. From idea to business – how Siemens bridges the innovation gap. Research-Technology Management 1999;42:26-31.

Schulder M, Azmi H, Biswal B. Functional magnetic resonance imaging in a low-field intraoperative scanner. Stereotact Funct Neurosurg 2003;80:125-131.

Scouten A, Papademetris X, Constable RT. Spatial resolution, signal-to-noise ratio and smoothing in multi-subject functional MRI studies. NeuroImage 2006;30:787-93.

Siegel AM, Roberts DW, Thadani VM, et al. The role of intracranial electrode reevaluation in epilepsy patients after failed initial invasive monitoring. Epilepsia 2000;41:571-80.

Stachó L, Dudás R, Ivády R, et al. [Addenbrooke's Cognitive Examination: developing the Hungarian version] Psychiat Hung 2003;18:226-40.

Talairach J, Tournoux P. Co-planar Stereotaxic Atlas of the Human Brain. Thieme, Stuttgart 1988.

Turner R, Jezzard P, Wen H, Kwong KK, Le Bihan D, Zeffiro T, Balaban RS. Functional mapping of the human visual cortex at 4 and 1.5 tesla using deoxygenation contrast EPI. Magn Reson Med 1993;29:277-279.

Uhlhaas PJ, Singer W. Neural synchrony in brain disorders: relevance for cognitive dysfunctions and pathophysiology. Neuron 2006;52:155-68.

Van Borsel J, Achten E, Santens P, Lahorte P, Voet T. fMRI of developmental stuttering: a pilot study. Brain Lang 2003;85:369-376.

Weber B, Fliessbach K, Lange N, Kugler F, Elger CE. Material-specific memory processing is related to language dominance. Neuroimage 2007;37: 611-617.

Weiskopf N, Sitaram R, Josephs O, Veit R, Scharnowski F, Goebel R, Birbaumer N, Deichmann R, Mathiak K. Real-time functional magnetic resonance imaging: methods and applications. Magn Reson Imaging. 2007 Jul;25(6):989-1003.

Wiebe S, Blume WT, Girvin JP, Eliasziw M, Effectiveness and Efficiency of Surgery for Temporal Lobe Epilepsy Study Group. A randomized, controlled trial of surgery for temporal-lobe epilepsy. N Engl J Med 2001;345:311-18.

Woermann FG, Jokeit H, Luerding R, Freitag H, Schulz R, Guertler S, et al. Language

lateralization byWada test and fMRI in 100 patients with epilepsy. Neurology 2003;61:699-701.

Yu CS, Li KC, Xuan Y, Ji XM, Qin W. Diffusion tensor tractography in patients with cerebral tumors: a helpful technique for neurosurgical planning and postoperative assessment. Eur J Radiol 2005;56:197-204.

Zald DH, Hagen MC, Pardo JV. Neural correlates of tasting concentrated quinine and sugar solutions. J Neurophysiol. 2002;87:1068-75.

8. List of own publications, presentations and posters

(cumulative IF: publications: 26.17; abstracts: 15.21)

The thesis is based on the following publications:

Auer T, Schwarcz A, Janszky J, Horváth Zs, Kosztolányi P, Dóczi T. [Application of functional MR-images acquired at low field in planning of neurosurgical operation close to an eloquent brain area] Ideggyogy Sz. 2007;60:35-40.

Schwarcz A, **Auer T**, Komoly S, Dóczi T, Janszky J. [Functional MRI at 1 Tesla. Basic paradigms and clinical application] Ideggyogy Sz. 2007;60:337-41.

Auer T, Schwarcz A, Ezer E, Czeiter E, Aradi M, Hudvágner S, Janszky J, Büki A, Dóczi T. [Diffusion tensor and functional MR imaging of severe traumatic craniocerebral injury at low magnetic field] Ideggyogy Sz. 2007;60:480-8.

Auer T, Schwarcz A, Horváth RA, Barsi P, Janszky J. Functional Magnetic Resonance Imaging in Neurology. Ideggyogy Sz. 2008;61:16-23.

Auer T, Schwarcz A, Doczi T,Merboldt KD, Jens Frahm J. A novel group analysis for functional MRI of the human brain based on a two-threshold correlation (TTC) method. J Neurosci Methods. 2008;167:335-9. IF: 2.243

Auer T, Vető K, Dóczi T, Komoly S, Juhos V, Janszky J, Schwarcz A. Identifying seizure onset zone and visualizing seizure spread by fMRI: a case report. Epileptic Disord. 2008;10(2):93-100. IF: 1.202

Kovács N, **Auer T**, Balás I, Karádi K, Zámbó K, Schwarcz A, Klivényi P, Jokeit H, Horváth K, Nagy F, Janszky J. Neuroimaging and cognitive changes during déjà vu. Epilepsy Behav. 2008;(Epub ahead of print) IF: 2.026

Schwarcz A, **Auer T**, Janszky J, Doczi T, Merboldt KD, Frahm J. TTC Post-Processing is Beneficial for Functional MRI at Low Magnetic Field: A Comparative Study at 1 T and 3 T. Eur Radiol. 2008;18(11):2594-600. IF: 2.556

The thesis is based on the following abstract:

Auer T, Schwarcz A, Dóczi T, Vető K, Juhos V, Janszky J. Visualization of seizure spread including activation and deactivation by ictal fMRI. Epilepsia 2006;47:36-68. Suppl 3. IF: 3.526

Kovács N, **Auer T**, Balás I, Karádi K, Zámbó K, Schwarcz A, Klivényi P, Jokeit H, Horváth K, Nagy F, Janszky J. Neuroimaging deja vu: An infrequent adverse reaction of pallidal deep brain stimulation. Movement Disord. 2008;23(1):67. Suppl.S. IF: 3.323

Kovács N, **Auer T**, Balás I, Karádi K, Zámbó K, Schwarcz A, Klivényi P, Jokeit H, Horváth K, Nagy F, Janszky J. Bilateral effects of unilateral thalamic depp brain stimulation: A neuroimaging study. Movement Disord. 2008;23(1):68. Suppl.S. IF: 3.323

Other publications:

Auer T, Schwarcz A, Aradi M, Kalmár Zs, Pendleton C, Janszky I, Horváth RA, Szalay Cs, Dóczi T, Komoly S, Janszky J. Right-left discrimination is related to the right hemisphere. Laterality 2008;13(5):427-38. IF: 1.364

Auer T, Barsi P, Bóné B, Angyalosi A, Aradi M, Szalay Cs, Horváth R, Kovács N, Kotek Gy, Fogarasi A, Komoly S, Schwarcz A, Janszky J. History of simple febrile seizures is associated with hippocampal abnormalities in adults. Epilepsia 2008;49(9):1562-9. IF: 3.526

Auer T, Pintér S, Kovács N, Kalmár Zs, Nagy F, Horváth RA, Koszó B, Kotek Gy, Perlaki G, Köves M, Kálmán B, Komoly S, Schwarcz A, Woermann FG, Janszky J. Does obstetric brachial plexus injury influence speech dominance? Ann Neurol. 2008; (accepted for publication) IF: 8.051

Bajzik G, **Auer T**, Bogner P, Aradi M, Kotek Gy, Repa I, Doczi T, Schwarcz A. Quantitative Brain Proton MR Spectroscopy Based on Measurement of the Relaxation Time T1 of Water. JMRI. 2008;28(1):34-8. IF: 2.637

Kellermayer R, Zsombok A, **Auer T**, Gallyas F. Electrically induced gel-to-gel phase-transition in neurons. Cell Biol Int. 2006;30:175-82. IF: 1.363

Tóth V, Rásonyi Gy, Fogarasi A, Kovács N, **Auer T**, Janszky J. Juvenile myoclonic epilepsy starting in the eighth decade. Epileptic Disord. 2007;9:341-5. IF: 1.202

Tóth V, Hejjel L, Kalmár Zs, Fogarasi A, **Auer T**, Gyimesi C, Szucs A, Janszky J. Effect of epileptic seizures on the heart rate. Ideggyogy Sz. 2008;61(5-6):155-61.

Other abstracts:

Auer T, Gallyas F. Electrically produced gel-to-gel phase transition in neurons. Ideggyogy Sz. 2005;58:198-215.

Czeiter E, Szellar D, Ezer E, Meszaros I, Kover F, **Auer T**, Schwarcz A, Doczi T, Buki A. Analysis of the Pecs severe traumatic brain injury database: The effect of guideline implementation on outcome. J Neurotraum. 2006;23(5):758. IF: 3.453

Deak A, Revesz G, **Auer T**, Doczi T, Janszky J, Schwarcz A. Neural correlates of viewing emotional stimuli. Perception 2007;36:135-135, Suppl. IF: 1.585

Presentations:

Auer T. Electric-shock experiments support the gel-to-gel phase-transition theory of the formation of "dark" neurons (whole-cell ultrastructural compaction). Házi TDK Konferencia, February 12, 2005, Pécs, Hungary

Auer T, Schwarcz A, Dóczi T, Vető K, Juhos V, Janszky J. Visualization of seizure spread including activation and deactivation by ictal fMRI. Magyar Epilepszia Liga Tudományos Ülése, May 25, 2006, Pécs, Hungary

Auer T, Schwarcz A, Vető K, Komoly S, Juhos V, Janszky J, Dóczi T. Identifying seizure onset zone and visualizing seizure spread in epilepsy by fMRI. Magyar Neuroradiológiai Társaság XV. Kongresszusa , October 26, 2006, Szeged, Hungary

Auer T. Post-processing and analysis of fMRI-data. MTA Magyar Tudomány Ünnepe: fMRI szerepe a kognitív és affektív folyamatok feltárásában. November 21, 2006, Pécs, Hungary

Auer T, Schwarcz A, Merboldt KD, Frahm J, Dóczi T. A novel group analysis for fMRI of the human brain based on a two-threshold correlation (TTC) method. Magyar Neuroradiológiai Társaság XV. Kongresszusa, October 25, 2007, Debrecen, Hungary

Auer T, Kovács N, Schwarcz A, Balás I, Zámbó K, Tasnádi E, Klivényi P, Jokeit H, Nagy F, Janszky J. Déjà vu elicited by pallidal deep brain stimulation: a Neuroimaging study. Magyar Neuroradiológiai Társaság XV. Kongresszusa, October 25, 2007, Debrecen, Hungary

Auer T, Schwarcz A, Janszky J, Dóczi T. FMRI-examinations in Pécs: What good is 1T magnetic field? Pécsi Akadémiai Bizottság – Neurobiológus Doktoranduszok Fóruma, November 16, 2007, Pécs, Hungary

Llumiguano C, **Auer T**, Kosztolányi P, Kovács N, Schwarcz A, Dóczi T, Balás I. 1H-MRS experiences after bilateral DBS of STN in Parkinson's Disease. The Movement's Disorders Society's 11th International Congress of Parkinson's Disease and Movement Disorders. June 3, 2007, Istanbul, Turkey

Posters:

Auer T, Gallyas F. Electric-shock experiments support the gel-to-gel phase-transition theory of the formation of "dark" neurons (whole-cell ultrastructural compaction). Magyar Idegtudományi Társaság Kongresszusa, May 28, 2005, Pécs, Hungary

Auer T, Gallyas F. Electrically produced gel-to-gel phase transition in neurons. CNS Injury International Symposium, April 30, 2005, Pécs, Hungary

Auer T, Gallyas F. Electric shock causes gel-to-gel phase-transition in neurons. Magyar Anatómiai Társaság Kongresszusa, June 18, 2005, Pécs, Hungary

Auer T, Schwarcz A, Dóczi T, Vető K, Juhos V, Janszky J. Visualization of seizure spread including activation and deactivation by ictal fMRI. 7th European Congress on Epileptology, July 2, 2006, Helsinki, Finland

Deak A, Revesz G, **Auer T**, Doczi T, Janszky J, Schwarcz A. Neural correlates of viewing emotional stimuli. 30th European Conference on Visual Perception, August 27, 2007, Arezzo, Italy

Deak A, **Auer T**, Revesz Gy, Janszky J, Schwarcz A, Doczi T. Arousal and valence-dependent brain activity responding to IAPS pictures. 1st DGPA Spring School 'The Biopsychology of Emotions', March 27, 2008, Kloster Seeon, Germany

Janszky J, Angyalosi A, Barsi P, Fogarasi A, Schwarcz A, **Auer T**. Simple febrile seizure I childhood and hippocampal MRI alterations in adulthood. Magyar Epilepszia Liga Tudományos Ülése, May 26, 2008, Pécs, Hungary

Szalay Cs, Schwarcz A, **Auer T**, Janszky J, Dóczi T, Hanna S, Rábai M, Karádi Z. Gustatory stimulation elicited changes in the human brain: an fMRI study. Magyar Idegtudományi Társaság Kongresszusa, January 24, 2007, Szeged, Hungary